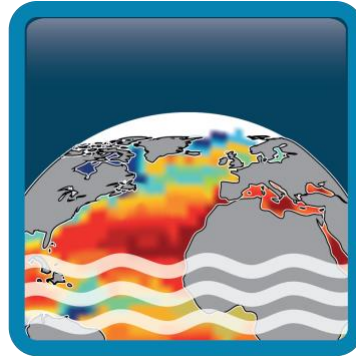


Climate Change Initiative+ (CCI+) Phase 1

Sea Surface Salinity



[D5.1] Climate Assessment Report (CAR)

Customer: ESA

Ref.: ESA-CCI-PRGM-EOPS-SW-17-0032

Version: v3.2

Ref. internal: AO/1-9041/17/I-NB_v1r2

Revision Date: 08/11/2021

Filename: SSS_cci-D5.1-CAR-v3.1_final.docx

Deliverable code: D5.1



Signatures

Author	Julia Koehler		
Reviewed By			
Approved By	Jacqueline Boutin (Science Leader)	LOCEAN	
	Nicolas Reul (Science Leader)	IFREMER	
	Rafael Catany (Project Manager)	ARGANS	
Accepted By	Susanne Mecklenburg (Technical Officer)	ESA	

Diffusion List
Sea Surface Salinity Team Members
ESA (Susanne Mecklenburg, Roberto Sabia, Paolo Cipollini)

Amendment Record Sheet

Date / Issue	Description	Section / Page
10-Jan 2020 / v1.0	Issue document to ESA	N/A
03-Apr-2020/v1.0	Reviewed document sent from ESA to Authors	
10-Apr-2020 /v1.1	Revision sent to ESA	All Document
	Addition of "Upper Ocean stratification in major Tropical Cyclone" (section 6.2.4.1	Section 6.2.4.1 / p. 30
	Addition of applicable and reference document lists	P. X, Xi
Nov 2020/v2.1	Version 2.1 sent to ESA	Section 3, 6 and 7
March 2021	Reviewed document sent from ESA to Authors	
April 2021	Revision sent to ESA	Section 2,3,6 Reference list Acronym list Table of figures
July 2021	Version 3.1 sent to ESA	
November 2021 / v3.2 (this doc)	Version to publish	NA

Table of Contents

Signatures	iii
Amendment Record Sheet	v
List of figures	vii
List of tables	x
Acronyms.....	xi
1 Introduction	15
1.1 Scope of this document	15
1.2 Structure of the document	15
2 User Requirements	16
2.1 What do users need?.....	16
2.2 How is CCI+SSS addressing the requirements?.....	18
2.3 How close are the products to GCOS Requirements?	19
3 Algorithm Development.....	20
4 Products.....	21
5 Validation of products against global in situ match-up data	23
6 SSS and climate variability.....	25
6.1 How well do we know ocean salinity and its changes?.....	25
6.2 Summary Salinity Science Seminar.....	29
6.3 Scientific Studies	29
6.3.1 CASE STUDY 3: Water cycle in the Bay of Bengal.....	29
6.3.2 Tropical Instability Waves in the Atlantic Ocean: investigating the relative role of sea surface salinity and temperature from 2010 to 2018.....	33
6.3.3 A fresh plume in the northwestern tropical Atlantic during the EUREC4A- OA/ATOMIC program in February 2020	36
6.3.4 CASE STUDY 2: Climate variability reconstruction in the Atlantic.....	37
6.3.5 CASE STUDY 4: Salinity stratification and small-scale variability	40
6.3.6 CASE STUDY 5: Comparing salinity variability between observations and models	54
6.3.7 CASE STUDY 1: North Atlantic salinity anomaly	58
6.3.8 Amazon river plume	65
6.3.9 SSS signatures related to ENSO	66
7 Summary and next steps.....	67
8 References.....	68

List of figures

Figure 3-1: Schematic of the CCI+SSS merging methodology. Satellite SSS data are indicated in light blue boxes, additional input information is in green boxes (origin of this information in bold black), processing steps are in yellow boxes and output CCI+SSS are indicated in purple boxes. 20

Figure 6-1 In situ ensemble mean of the long-term mean salinity (2004-2017, left), and the ensemble spread of this mean (right), at the surface, i.e., at 5 m depth, vertically averaged in the layers 10 to 50 m, 50 to 300 m and 300 to 700 m, respectively. The color scale of the right panels is logarithmic to enhance the visibility. ----- 27

Figure 6-2 Ensemble-mean annual amplitude in salinity variability of the ensemble in situ data, at (a) 5 m depth and (c) in the layer averaged from 5 to 50 m. Ensemble spread of the annual amplitude in percent relative to the total amplitude at (b) 5 m depth (d) and 50 m depth layer. ----- 28

Figure 6-3: Bay of Bengal SSS from the CCI product in November 2015 (left) and 2016 (right). With very strong salinity contrasts due to large freshwater inputs and an energetic circulation, the Bay of Bengal is a good laboratory to monitor large salinity signals. Here, the very fresh waters associated with the Irrawady and Ganges-Brahmaputra estuaries are strongly influenced by mesoscale eddies and the interannual variability. The opposite polarities of the “Indian Ocean Dipole” climate mode in 2015(IOD+) and 2016 (IOD-) result in a clear southward East Indian Coastal Current in 2016, and the Ganges-Brahmaputra freshwater plume extends further southward along the India coast that year ----- 30

Figure 6-4 2010-2020 time series for a) the average September-November value of the DMI (Dipole Mode Index, and index of the IOD) with positive events marked in red and negative ones in blue; b) SSS within 100 km of the east coast of India (Southward EICC occurrences are marked by the black contours) and c) as b but for SSS anomalies with respect to the 2010-2020 mean seasonal cycle. ----- 32

Figure 6-5: Snapshot of SSS (upper panel) on the 5th of June 2017 showing the deformation of the SSS front at 1°N by tropical instability waves. (Lower panel) Snapshot of band pass filtered SSS data (20-50 day band pass filter, 20° longitude high pass filter)----- 34

Figure 6-6: Hovmöller diagram of the sea surface salinity anomalies (SSSA, left), SST (middle) and sea level anomaly (SLA, right) at 1°N over the period January 2010 to December 2018 . --- 34

Figure 6-7 5th June 2017 snapshot of a) sea surface salinity, b) sea surface temperature, c) sea surface density ($\sigma = \text{density} - 1000 \text{ kg/m}^3$), d) surface chlorophyll. ----- 35

Figure 6-8:CCI+SSS daily snapshots of a fresh plume in the northwestern tropical Atlantic from 2012 to 2019.----- 37

Figure 6-9 Evolution of the AMOC at 48° N for global SST and global SSS (Glob-Full in yellow), limited to 45° in both hemispheres (45N-45S in red), limited to 60° in both hemispheres (60NSPG-60S in blue) and control runs (Control in grey). Numbers in the labels indicate correlation and root mean square error of each experiment with the Target over the 100 years. 99 % confidence level of correlation is indicated as **. ----- 39

Figure 6-10: Evolution of the AMOC at 48°N for global SST and global SSS (Glob-Full in yellow), perturbed with a white noise 0.2 (WN0.2psu in blue) and control ensemble (Control in grey).

Numbers in the labels indicate correlation and root mean square error of each experiment with the Target over the 100 years. 99 % confidence level of correlation is indicated as **.----- 40

Figure 6-11: Averaged relationships between (a) SSS, (b) SST, and the maximum buoyancy frequency N_{max} determined below the surface from ARGO floats within the Amazon and Orinoco river plume extent ($[78^{\circ}W-25^{\circ}W; 5^{\circ}S-30^{\circ}N]$) over 2010-2018. Linear fits are indicated by black and blue solid lines. The average values of SSS and SST are given by the dotted lines per N_{max} value bins of width 2.5 cph. ----- 42

Figure 6-12 (a ,c, e,g, i) Time series of CCI (blue) and CMEMS-Mercator model (red) SSS spatially averaged at the mouth of 4 major tropical river plumes (a: Mississippi River Mouth, c: Amazon River Mouth, e: Orinoco River Mouth, g: Congo River Mouth and i: Ganges/Brahmaputra River Mouth). b,d,f,h,j,: Time series of CCI (blue) and CMEMS (red) model SSS and river discharge (black) scaled anomalies (obtained by subtracting the record mean value from individual value). Scale factors are indicated in the legend. ----- 47

Figure 6-13 CCI+SSS on 30 June 2011 with 93 TSG transects in the Subtropical North Atlantic (dashed) and 26 TSG transect in the Tropical Atlantic (solid lines). ----- 49

Figure 6-14 a) Density spectra from 88 co-located TSG (black); CCI+SSS v2.31 (dashed red); CCI+SSS v3.1 (solid red) SSS transects in Subtropical North Atlantic. Vertical thick black bar is the level of confidence at 95%. b) Coherency between the TSG and CCI+SSS SSS transects. Dashed line is the level of significance at 95%. c) Density spectra from from 26 colocated TSG(black)/CCI+SSS(red) SSS transects in Tropical Atlantic. Vertical thick black bar is the level of confidence at 95%. d) Coherency between the TSG and CCI +SSS SSS transects. Dashed line is the level of significance at 95%. ----- 51

Figure 6-15: Scatter plot of TSG SSS measurements (a) and Argo/CTD data (b) with the CCI+SSS v2.31 products in the Gulf of Guinea ($15^{\circ}S-10^{\circ}N/10^{\circ}W-15^{\circ}E$) over the period 2010-2019. (c) distribution of the difference of co-located in situ/CCI+SSSv2 (in pss) as a function of the distance from the coast.----- 53

Figure 6-16: (a) Correlation of satellite CCI+SSS v3.2 and uppermost ENS salinity. (b) Ratio of the annual amplitude of the difference between satellite CCI+SSS v3.2 and ENS uppermost salinity and the annual amplitude of the ENS uppermost salinity. (from Stammer et al., 2020)----- 54

Figure 6-17: Amplitude of the annual cycle of (a, b) salinity tendency (ST), (c, d) surface external forces (SEF), (e, f) mean horizontal salinity advection (mean HADV), (g, h) entrainment (ENTR) and (i, j) vertical salinity diffusion (VDIFF), for (left) the model over the period 1980–2009 and (right) the CCI+SSS v3.2 observations in the period 2011–2019. ----- 56

Figure 6-18: Percentage of the MLS tendency annual variance explained by (a) surface external forces (SEF), (b) mean horizontal advection (mean HADV), (c) entrainment (ENTR), (d) vertical diffusion (VDIFF) and (e) the sum of the considered terms (SEF + mean HADV + ENTR + VDIFF), using model data. Locations with explained variance less than 5% are masked white. ----- 58

Figure 6-19 Difference of CCI+ SSS between 2014-17 and 2010-13. ----- 59

Figure 6-20: Difference of CCI+SSS linear salinity trend fields (pss/yr). Note positive values in North Atlantic mid-high latitudes. ----- 59

Figure 6-21: Salinity anomalies (with respect to 2010-2017) in the North Atlantic before and after the trend adjustment. Note circled fresh anomaly which is more evident following the trend correction. ----- 60

Figure 6-22: Monthly salinity anomalies relative to the monthly climatology computed from May 2015 to December 2019 in the North Atlantic for June, July and August, September and October 2018 and 2019 for (upper two rows) CCI+SSS and (lower two rows) ISAS. ----- 61

Figure 6-23: Monthly EN4.2.1 salinity anomalies (with respect to 1981-2010) in the North Atlantic in 2018. ----- 62

Figure 6-24: Monthly EN4.2.1 salinity anomalies (with respect to 1981-2010) in the North Atlantic in 2019. ----- 63

Figure 6-25: Hovmöller diagram showing EN4.2.1 monthly salinity anomaly at 5 points along the propagation track.----- 64

Figure 6-26 : Time series of the mean Sea Surface Salinity in different boxes along the path of the Amazon river plume, in red the Mercator Ocean global 1/12° analysis and in blue the ESA CCI+ weekly L4 SSS (v1.8). Top right panel: mean SSS in the small box close to the river mouth, bottom left panel in the second box (6°N-13°N) and bottom right panel in the largest box covering the Caribbean archipelago.----- 65

Figure 6-27 Zonal month-longitude cross sections (averaged 5°S and 5°N) for Sea Surface Salinity (CCI+SSS v2.3) ----- 66

List of tables

Table 2-1 GCOS in situ sea surface salinity requirements reproduced from GCOS 2016 Implementation Plan: The Global Observing System for Climate: Implementation Needs ----- 19

Acronyms

AD	Applicable document
ADB	Actions database
AMOC	Atlantic Meridional Overturning Circulation
ATBD	Algorithm theoretical basis documents
BRO	Brochure
CLiC	Climate and Cryosphere
DIR	Directory
DS	Dataset availability
DS-UM	Dataset user manual
DVP	Development and validation plan
EC RTD	European Commission Directorate General for Research and Innovation
EDS	Experimental dataset
EMI	Electromagnetic Interference
EO	Earth Observation
EOEP	Earth Observation Envelope Program
ESA	European Space Agency
FR	Final review
FWF	Freshwater fluxes
GCOS	Global Climate Observing System
IAR	Impact assessment report
ITT	Invitation to tender
IPP	Year of Polar Prediction
KO	Kick-off
MR	Monthly report
MTR	Mid-term review
MV-TN	Modelling and validation technical note
NDVI	Normalized Difference Vegetation Index
PAR	Preliminary analysis report
PGICs	Peripheral glaciers and ice caps
PM	Progress meeting
PMP	Project management plan
RD	Reference document
RB	Requirements baseline
SAR	Synthetic Aperture Radar
SIAR	Scientific and impact assessment report
SMOS	Soil Moisture and Ocean Salinity
SoW	Statement of work
SR	Scientific roadmap

SSS	Sea Surface Salinity
SST	Sea Surface Temperature
TDP	Technical data package
TDS	Training Data Set
TN	Technical note
VIR	Validation and intercomparison report
VR	Validation report
WCRP	World Climate Research Programme
WP	Work package
WS	Workshop minutes
WWRP	World Weather Research Programme
AD	Applicable document
ADB	Actions database
AMOC	Atlantic Meridional Overturning Circulation
ATBD	Algorithm theoretical basis documents
BRO	Brochure
CLiC	Climate and Cryosphere
DIR	Directory
DS	Dataset availability
DS-UM	Dataset user manual
DVP	Development and validation plan
EC RTD	European Commission Directorate General for Research and Innovation
EDS	Experimental dataset
EMI	Electromagnetic Interference
EO	Earth Observation
EOEP	Earth Observation Envelope Program
ESA	European Space Agency
FR	Final review
FWF	Freshwater fluxes
GCOS	Global Climate Observing System
IAR	Impact assessment report
ITT	Invitation to tender
IPP	Year of Polar Prediction
KO	Kick-off
MR	Monthly report
MTR	Mid-term review
MV-TN	Modelling and validation technical note
NDVI	Normalized Difference Vegetation Index
PAR	Preliminary analysis report

	<p><i>Climate Change Initiative+ (CCI+)</i> <i>Phase 1</i> Climate Assessment Report</p>	<p>Ref.: ESA-CCI-PRGM-EOPS-SW-17-0032 Date: 08/11/2021 Version : v3.2 Page: 15 of 75</p>
--	--	--

1 Introduction

1.1 Scope of this document

This document presents a climate assessment of the European Space Agency Sea Surface Salinity Climate Change Initiative (ESA CCI+SSS) Phase 1 products (version 1 and version 2). The document describes the results of the usage and application of the CCI+SSS project sea surface salinity data sets in climate research – namely for inter-comparison to model data and for usage in assimilation experiments. It also describes results from using the CCI+SSS data sets for estimation of salinity changes. The document also includes comparisons of the products to other salinity data sets.

1.2 Structure of the document

After the introduction the document is divided into several major sections that are briefly described below:

Section 1 is an introduction, describing the background and scope of the project.

Section 2 presents a summary of the user requirements.

Section 3 gives a short overview about the algorithm development; Section 4 is dedicated to the description of the existing data sets, up to v3. In Section 5, an overview of the validation procedures against in-situ data and related metrics is given.

Section 6 presents an assessment of trends and variability in the CCI+SSS data products and detailed analysis of the data in the framework of five different case studies also including a summary of assimilation and model studies from climate scientists and an overview of additional scientific studies.

Further details about section 2 to 5 can be found in Boutin et al. 2021, and in dedicated CCI+SSS technical reports.

	<p style="text-align: center;">Climate Change Initiative+ (CCI+) Phase 1</p> <p style="text-align: center;">Climate Assessment Report</p>	<p>Ref.: ESA-CCI-PRGM-EOPS-SW-17-0032 Date: 08/11/2021 Version : v3.2 Page: 16 of 75</p>
--	--	--

2 User Requirements

The first step is to generate the user requirements and the product specifications that drive the further technical developments by compiling and maintaining ECV user requirements through user consultation activities (including the climate modelling community), product specification and data requirements documentation. This implies to survey, update and verify detailed user requirements (i.e., performance, coverage, spatial resolution, uncertainty limits, provision and application, format, data latency, documentation, validation metrics, applications etc.) for climate science research and climate services, elaborating on the high-level requirements specified by GCOS. During the course of this process, we assist users in understanding the advantages and limitations of satellite retrieved SSS products in the context of their specific applications. The survey also aims at obtaining feedbacks from climate users on the performance (i.e., validation and impact in applications) of the SSS products provided. This is achieved through a combination of engagement with key climate science research and modelling groups (e.g., CMUG), interaction with other European and national projects and international bodies, as well as individual or institutional bilateral contacts.

2.1 What do users need?

A user requirement survey was conducted with the goal to identify the requirements of SSS data for climate studies at present and in the future. The “satellite and in situ salinity (SISS)” working group discussions at several conferences (e.g., WHOI 2017, OSM 2018, Salinity Conference Paris 2018) were useful in focusing on the main issues to be addressed in the CCI+SSS survey.

Users were consulted through various approaches, personally via email, via mailing lists, or at meetings (e.g., CMUG meeting Oct. 2018, Salinity Science conference, Paris Nov 2018). Respondents participated in a web-based (Google Forms) survey or completed the survey offline via printouts. The members of the CCI+SSS working groups were requested to distribute the survey widely to colleagues. To promote the actions of the CCI+SSS working group and to discuss the requirements of the specific user groups, team members participated in several meetings with modelers, data assimilation scientists etc. and conferences. These opportunities were also used to spread the survey.

Users were contacted in year 1 and 2 to refine the requirements and check the satisfaction with the CCI+SSS products. In year 2 users participated in a live survey (VoxVote) during the Hamburg Salinity Science Seminar (26/27 September 2019) or participated in a web-based survey.

Current and future users of satellite SSS data were invited to participate in a web-based survey and enter their requirements for satellite SSS data. 54 responses were analysed in total.

The results of the questionnaire have been published, every single question was evaluated and discussed. Wide ranges in responses were received for many questions, indicating that there is no single product that will satisfy everyone.



The survey revealed that the majority of users require global spatial coverage and a temporal coverage from at least 9 years. The resolution requirements vary according to the studied phenomena. About 33% of respondents' want data with a temporal resolution of 1-3 days, while for 35% of the respondents' weekly data and for 28% also monthly data are sufficient. 39% of the respondents want data with 0.25° spatial resolution, for 28% data on a 1°-grid are sufficient. The majority of respondents would prefer a data product with high spatial and temporal resolution (weekly, 0.25°) on a regular latitude longitude grid and would accept a lower accuracy (approx. 0.3).

The results are discussed in the user requirement document (URD, <https://climate.esa.int/>). To summarize, the requirements of the participants are not substantially different from the GOOS requirements and former user requirement studies. The World Meteorological Organization (WMO) summarizes SSS requirements from salinity data users for various applications, which can be viewed under: https://www.wmo-sat.info/oscar/variables/view/sea_surface_salinity. These correspond to the requirements discussed above. All in all, required are data product resolutions and coverage dependent on the users' application category. The users are aware of the possibility that this data offer and that a high spatial/temporal resolution also influences the accuracy of the data. In our survey we asked the questions to find out what is more important for the user, the high resolution or the higher accuracy with the result that users would prefer a data set with a higher spatial and temporal resolution. These requirements are met with the datasets produced by the CCI+SSS team.

Data should be combined to overcome weaknesses in individual datasets: here, 50% prefer a combination of satellite and in situ measurements, whereas 39% require the combination of data from different satellite sensors. In situ data were used for calibration and validation of the satellite data as well as for the analysis of physical processes described in the case studies (Section 6).

By making available the multiple-sensor datasets on different spatial-temporal grids, the needs of different users can be met. The most common requirement is for L4 data (43%), directly followed by requirements for L3 (37%). Some potential users, mainly modelers, require L2 (20%). L3 and L2 data are already available from ESA, CATDS, BEC, RSS and JPL and were not the main focus of the CCI+SSS project during the first phase of the project. In the next years also de-biased L2 and possibly L3 products will be made available, to satisfy the requirements of some users.

Uncertainty information for each SSS grid point needs to be characterized fully, including random noise and systematic errors and uncertainties of applied adjustments. Information about bias correction is most commonly required by respondents. 50% of respondents want to have flags for each/selected quality control checks, which is not possible for datasets at L3 or L4, which are already binned. Therefore, quality information is needed for each SSS value that is simple to use, such as good/bad flag or the probability that a value is good/bad. 46% of the respondents would prefer such a solution for quality information. Participants indicated how important a detailed documentation is, both in the multiple-choice questions and when asked what is expected from the new CCI+SSS product.



Data need to be easily accessible; a majority of respondents (94%) require data in NetCDF, accessible via FTP server (81%), followed by a webpage (6%) and OpenDAP (6%). Updates/News/Alerts should be communicated via email (81%) followed by web page (17%) and this continuous at least once a year (28%, all in all 57% more often).

The most common service that the respondents wish to have provided is a simple documentation, followed by a detailed documentation. The tools that respondents would like the CCI+SSS project to provide are primarily data extracting and reading tools. Respondents choose MATLAB (54%) as most common choice as language for software libraries, followed by Python (28%) and FORTRAN (11%).

User Requirement Survey Year 1 and 2 results show the importance of contacting users and promote communication between the project, users, and potential users. Large changes in user requirements of spatial-temporal resolution and coverage are not expected soon, but users should be contacted regularly to refine requirements, to check the satisfaction with the CCI+SSS product and to reach (climate) community acceptance of SSS as an ECV. The recommendations derived from the user consultation are transformed into a set of product specifications for input into Task 2 of the CCI+SSS project (Product Specification Document (PSD), SSS_cci-D1.2-PSD-v1r4.docx).

2.2 How is CCI+SSS addressing the requirements?

The survey conducted by the project was very detailed and the requirements are widely spread. Therefore, not all aspects of user requirements are covered by the first phase of CCI+SSS (which coincides with the third programmatic phase of the whole CCI Program).

The goal is to design products that meet as many requirements as possible considering the available options. The recommendations derived here from the user consultation relate to the need for a growing and diverse user community and their needs:

- **Make high-resolution data available** to account for the high diversity of requirements for spatial-temporal resolution of the products. The survey results show that the resolution needs to strongly depend on the analysed phenomena, ranging from original spatial sampling to 10° and temporal resolution from weekly (daily sampling) to monthly (15-day sampling).
- **Uncertainty specification for L4 SSS product, along with uncertainty estimation details**, to account for the need of broad uncertainty specification. The CCI+SSS L4 product contains an estimated uncertainty, as well as good/bad flags computed from different indicators (Xi2, number of outliers). Systematic uncertainty, that is removed from the final product, is kept in L3 products but is not included in L4 version 3 products to avoid confusion and following recommendations of users of L4 versions 1 and 2 data.
- **Compatibility between products (L2, L3, L4, other CCI products)**



2.3 How close are the products to GCOS Requirements?

SSS observation requirements have been defined by the GCOS Physics and Climate Panel in their latest document (GCOS 2016 Implementation Plan). It is recommended there that the continuity of space borne SSS measurements must be ensured (Action O32, GCOS 2016 Implementation Plan).

The GCOS requirements for the ECV SSS are listed in Table 2-1. We note, however that at the moment, the GCOS requirements cannot be met with in situ and/or satellite measurements. In 2021, CMUG also formulated requirements for SSS data, which are close to the GCOS requirements. At this stage, these requirements cannot be met with satellite retrieved sea surface salinities. An accuracy (random component of the uncertainty) of 0.01 is even difficult to meet with in situ salinity data.

In the last year of Phase 1 and at the beginning of Phase-2 CCI+SSS plans to bring modelers and Earth observation scientists on one table to put together ideas of how to define the user requirements for SSS to fulfil some of the modeler's requirements, e.g., what exactly is needed for various applications, to identify requirement goals and thresholds and to clarify for what purpose satellite-retrieved salinity data are/ can be used in modelling/assimilation studies. Furthermore, results of a new survey organized by GCOS will be published in 2022.

Table 2-1 GCOS in situ sea surface salinity requirements reproduced from GCOS 2016 Implementation Plan: The Global Observing System for Climate: Implementation Needs

Variable	Frequency	Horizontal resolution	Required measurement uncertainty	Stability/Decade
SSS	hourly to monthly	1-100 km	0.01	0.001

3 Algorithm Development

For each CCI+SSS version, we consider the longest SMOS, SMAP and Aquarius SSS time series available at the time of the development of each CCI+SSS data set.

The merging of the three existing satellite data sets is performed after standardizing the error estimation by using self-consistency criteria: by comparing SSS acquired at the same time by different sensors, we extract systematic uncertainties and random errors on SSS from each satellite mission. They are used to correct individual SSS before merging using a temporal OI and to estimate the final uncertainty on level 4 (L4) SSS.

The algorithm is summarized on *Figure 3-1*. It is described in detail in the ATBD.

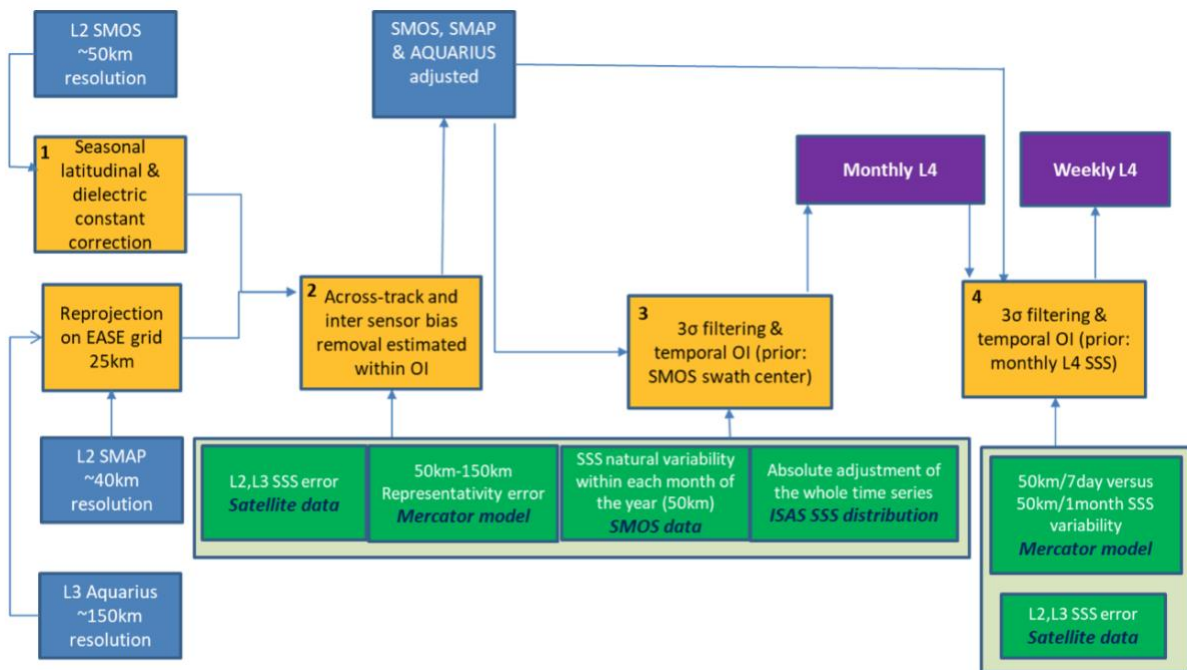


Figure 3-1: Schematic of the CCI+SSS merging methodology. Satellite SSS data are indicated in light blue boxes, additional input information is in green boxes (origin of this information in bold black), processing steps are in yellow boxes and output CCI+SSS are indicated in purple boxes.

The various corrections applied to satellite SSS are relative. As a result, SSS anomalies are available at the end of the OI processing. These anomalies are then calibrated against an absolute reference. This shift is a time-independent correction in order to maintain the temporal dynamics observed by the satellite measurements: a quantile of 8year long SSS statistical distribution obtained with CCI+SSS and ISAS is adjusted in each pixel. Other information than satellite data considered by the L4 algorithm is climatology of representativity errors that are derived from Mercator model.

	<p style="text-align: center;"><i>Climate Change Initiative+ (CCI+)</i> <i>Phase 1</i></p> <p style="text-align: center;">Climate Assessment Report</p>	<p>Ref.: ESA-CCI-PRGM-EOPS-SW-17-0032 Date: 08/11/2021 Version : v3.2 Page: 21 of 75</p>
--	---	--

4 Products

The SSS ECV products v3.2 consist of two Level-4 datasets from January 2010 to December 2020:

- A monthly mean product centred on the 1st and 15th day of each month.
- A 7-day running mean at one-day time sampling

Input data used to produce the dataset are SMOS level 1, SMAP level 2 and Aquarius level 3 (L2 like, daily, ascending and descending passes separately) . SMOS SSS has been reprocessed with the CCI processing chain from ESA L1c data. SMAP and Aquarius L2/L3 products have been taken from the space agency dedicated centres; their uncertainties have been qualified by the CCI processing chain. Data are the following for each sensor:

- SMOS ESA L1c v6 processed with v662 L2OS processor with the main following CCI adjustment:
 - ISAS SSS for computing Ocean Target Transformations (OTT); OTTs are centered in time
 - ECMWF ERA5 fields instead of ECMWF IFS (forecasts) fields (wind, SST, atmospheric parameters) as prior auxiliary fields in the retrieval scheme
 - Boutin et al (2020) instead of Klein and Swift (1977) dielectric constant model
- Aquarius Level 3 SSS produced daily for ascending and descending passes separately with version v5.0
 - A spatial interpolation gaussian kernel instead of nearest neighbor (to avoid abrupt spatial discontinuities between point measurements) has been applied
- SMAP Level 2 SSS produced with RemSS version v4.0

To build the L4-products, external information other than the satellite signal are as much as possible limited.

The external information used to build the L4 SSS products as well as the L2 SSS entering the L4 products are the following:

- CCI L4 algorithm:
 - Representativity error derived from Mercator model (monthly climatology)



- In each pixel, adjustment of absolute SSS value using 8 year median ISAS SSS (or 8-year high quantile of ISAS SSS distribution in highly variable areas)
- Individual sensor calibration:
 - SMOS – ***no geographical dependency***: Ocean Target Transformation (OTT): Mean SMOS Tb in a SE Pacific Ocean box (45S-5S) over ~10days adjusted to mean modelled Tb derived from ISAS.
 - Aquarius – ***no geographical dependency***: Ocean Target Calibration (OTC): Mean global Aquarius Ta adjusted every 7day to mean global Ta derived from Scripps-Argo (or Hycom if Argo not available)
 - SMAP – zonal dependency - emissive reflector correction to minimize orbital biases, estimated for each day of the year using Scripps Argo SSS. It is the same for all years (Meissner et al., 2019). Spatially constant and time-varying mean calibration: OTC: 3day mean differences over global ocean using Hycom SSS (Meissner et al., 2019).

These data are all projected on the same EASE2 cylindrical equal area grid at a spatial sampling of 25 km (584x1388 grid points). In each grid point, based on the internal consistency of the SSS temporal variability measured by each sensor, an adjustment of their systematic errors is estimated following a procedure like the one described in Boutin et al. (ESSOAR 2021). This procedure allows to retrieve SSS variability over 10years relative to an arbitrary reference. The CCI+SSS adjustment depends on SMOS and SMAP measurement geometry and on SSS natural variability as inferred from Mercator Ocean model. The CCI+ SSS is derived using a temporal optimal interpolation. The product complies with the latest version of the CCI Data Standard requirements [DSTD] and includes, beside the SSS field, random and systematic error, and their variability as well as quality information.

This first version (v1.8) of the CCI+SSS products was a preliminary version issued for evaluation purposes by voluntary scientists and for framing future CCI+SSS products. Version v2.3 is available since September 2020. Version 3 has been made publicly available on CEDA in September 2021 (DOI: [10.5285/5920a2c77e3c45339477acd31ce62c3c](https://doi.org/10.5285/5920a2c77e3c45339477acd31ce62c3c))

The CCI+SSS products are described in the Product User Guide (PUG). The algorithms used to obtain the products are described in the Algorithm Theoretical Basis Document (ATDB) and the production chains used are explained in the Detailed Processing Model (DPM) document. The Product Validation and Intercomparison Report (PVIR) describes the results of the evaluation efforts. Data used for some of the inter-comparison studies found in this report are given in the DARD.



5 Validation of products against global in situ match-up data

Climate users of satellite retrieved SSS data products need to know detailed uncertainty qualification of any products. Ideally this should be provided as error covariances. However, the whole set of error covariances are not provided because of data volume issues.

Uncertainties in the SSS products can arise due to many aspects that we grouped here into the following primary categories (see Product Validation Protocol (PVP):

- instrument measurement uncertainty: those relating to instrument hardware
- retrieval/algorithm uncertainty: those relating to derived quantities
- application uncertainty: those relating to a specific application
- unknown uncertainties

A detailed documentation of random and systematic uncertainties in the available SSS product as well as a documentation of their calculation is described in the ATBD and E3UB documents.

A detailed description of the associated global validation of the SSS product can be found in the PVIR. Here only the main results are highlighted.

The main validation results for version v2.3 are the following:

- In situ reference data are Argo floats upper salinity measurement between 0 m and 10 m, which is the only dataset uniformly distributed over the globe.
- Need to take robust estimator (based on the data distribution: median, standard deviation estimated from a ratio to IQR, ...) to be robust to non-normal distribution and fairly representative of the behaviour of more than 50% of the observations
- No systematic bias against reference data evidenced (see PVIR)
- Global precision against reference data is of 0.15 (see PVIR)
- CCI version 2 products show similar performance than v1 but is one year longer and provide access to individual satellite and passes
- Coherent variability between CCI and in situ data
 - more coherent small-scale high-frequency variability for CCI
 - coherent annual amplitude signal
 - larger amplitude in the inter-annual variability for CCI



- Good agreement between CCI and reference data, including long-term stability, differences within ± 0.05 for latitudinal band between $[40^{\circ}\text{S}-20^{\circ}\text{N}]$

Strong seasonal oscillation of CCI SSS differences against reference:

- CCI are fresher/saltier in Winter/Summer than reference
- Amplitude is maximum at high latitudes (40° - 60°) and can exceed 0.1 peak-to-peak
- Amplitude is stronger for L3 SMOS
- CCI SSS is higher than reference data in the beginning of the time series (2010) up to 2012 with an amplitude up to 0.1
- CCI data in the Arctic and Southern Ocean have not been properly validated as there are limited suitable in situ references
- Uncertainty observations and estimates agree within $\pm 25\%$, excepted for Aquarius which is generally underestimated



6 SSS and climate variability

Salinity is a key ocean variable that plays a fundamental role in the density-driven global ocean circulation, the water cycle, and climate (Siedler et al., 2001). The Sea Surface Salinity measurement by satellite remote sensing has been initially motivated by the essential need of better monitoring, understanding and constraining the marine component of the water cycle and ocean circulation. SSS is an ECV (Essential Climate Variable). In the frame of the CCI+SSS project, the CCI+SSS products and model results are analysed both spatially and temporally as well as in terms of consistency of results with other ECV products. For this purpose, five case studies are performed. In each of the five case studies, a different and complementary type of product assessment is conducted to assess the usefulness of sea surface salinity data as well as the CCI+SSS data product quality and its appropriateness for climate models. This is complemented by an additional set of scientific studies exploring further the CCI+ SSS products information content in a wider climate sense. All available data sets are used together to investigate the salinity variability over the Atlantic, but also the Indian Ocean and Pacific. The CCI+SSS data are compared with the existing knowledge from in situ and model data about the changing ocean, and differences are interpreted in terms of physical signal but also in terms of error structures. The assessment of output of the CCI+SSS system has been performed by members of the CCI+SSS community in close cooperation with other CCI projects. Results served and will serve to provide feedback to the project team responsible for the SSS ECV product generation to aid algorithm improvement. These activities help to quantify the added value of ECV dataset generated in terms of improvement over existing provision. Detailed regional validation aspects are highlighted in the PVIR document for the different case study regions.

First, we summarize how well we know ocean salinity and its changes by comparing various existing data sets against each other as well as against existing ocean reanalyses and the CCI+SSS data set (Stammer et al., 2021). Second, a (first) assessment of salinity variability on various timescales and trends is presented and which additional information we can obtain with the new CCI+SSS data. For this, five case studies have been performed as well as scientific studies from outside of the project. The studies are sorted by climate relevance and the case studies are marked.

6.1 How well do we know ocean salinity and its changes?

Stammer et al. (2021) established an understanding of the consistency among existing salinity products and quantified remaining uncertainties by comparing a variety of salinity products against each other. Focusing on the large-scale salinity structures of the top 700 m, they find that all existing climatological data sets reproduce the major well-known structures of the salinity climatology, notably the subtropical salinity maxima, the relative salinity minima in the upper layer of the tropics and especially around the maritime continent, and lowest salinity in the subpolar regions. Associated uncertainties as measured by the spread among the climatologies are as large as 0.3 within the first 50 m of high vertical salinity gradients and even larger in some



boundary regions. Away from boundaries, a near-surface spread of 0.1 can be observed. However, below 300 m depth, the spread stays below 0.03 over most part of the world ocean. Note, that in the presence of inter-decadal and longer-term salinity variability, the time-mean and variability of salinity climatologies, established primarily based on recent Argo measurements, do not provide an accurate long-term estimate. Near the surface related inter-decadal variability could add about 30% of the magnitude of the ensemble spread and could substantially add to the uncertainty.

Are existing salinity data sets, including satellite products, skillful in describing salinity changes? Highest salinity variability occurs in the surface layer in regions of highly variable precipitation and river runoff, but also in frontal regions; at greater depths enhanced variability is primarily confined to frontal regions, such as the North Atlantic Current or the Agulhas region. Using again the difference between climatologies as measure of uncertainty, we find that in the upper 50 m the spread of the total variability essentially stays below 30% of the signal over most of the world ocean (compare Figure 6-1).

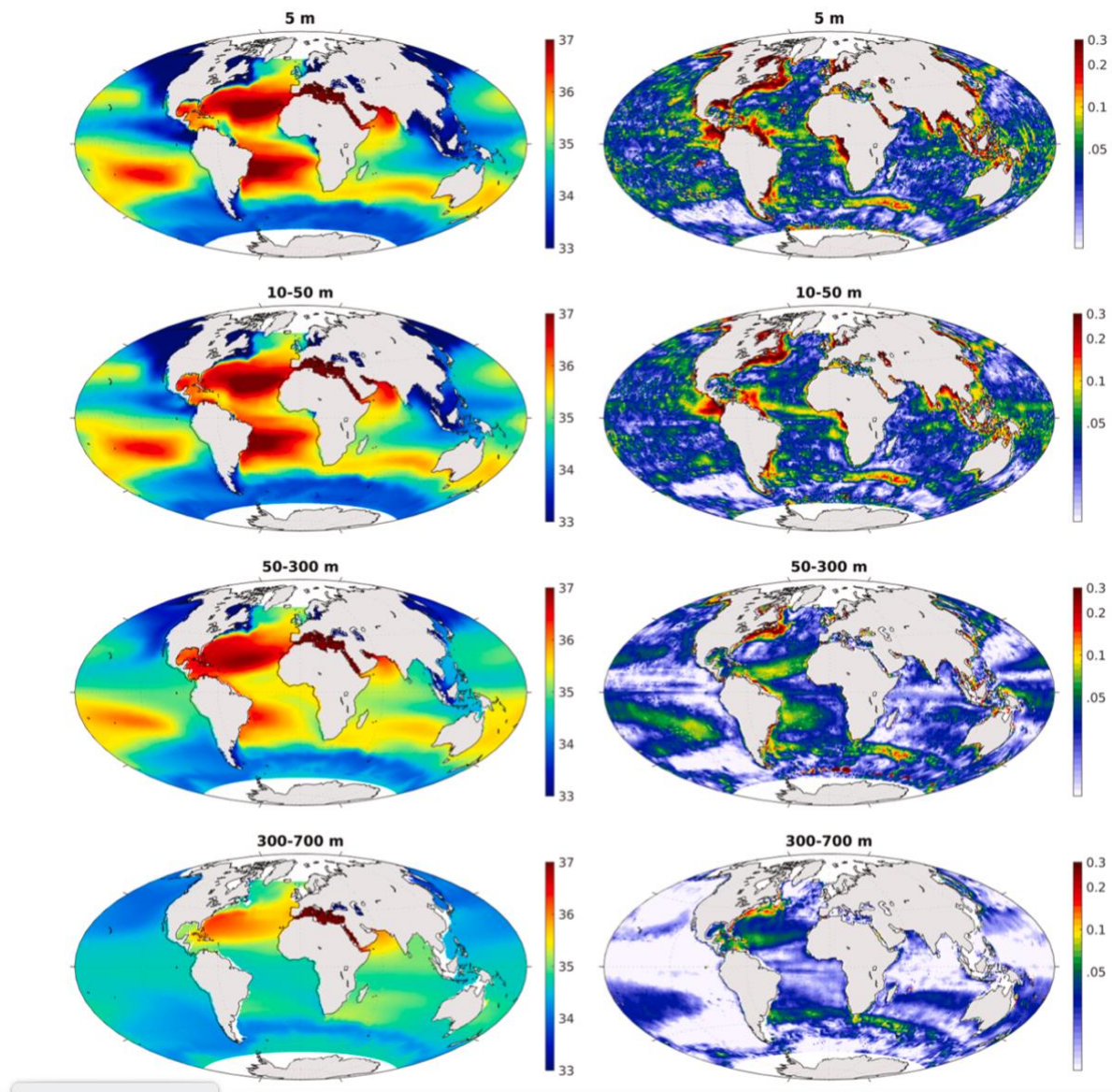


Figure 6-1 In situ ensemble mean of the long-term mean salinity (2004-2017, left), and the ensemble spread of this mean (right), at the surface, i.e., at 5 m depth, vertically averaged in the layers 10 to 50 m, 50 to 300 m and 300 to 700 m, respectively. The color scale of the right panels is logarithmic to enhance the visibility.

Only in a few “hot spots” it increases, marking especially regions around islands or selected coastlines. In contrast, below 50 m depth the variability uncertainties generally exceed 50% over large parts of the world ocean, documenting an enhanced disagreement between data products in describing salinity changes (variability and trend) there and calling for much improved salinity data sets, especially as some of the regions with enhanced uncertainty are those which remain severely under sampled.

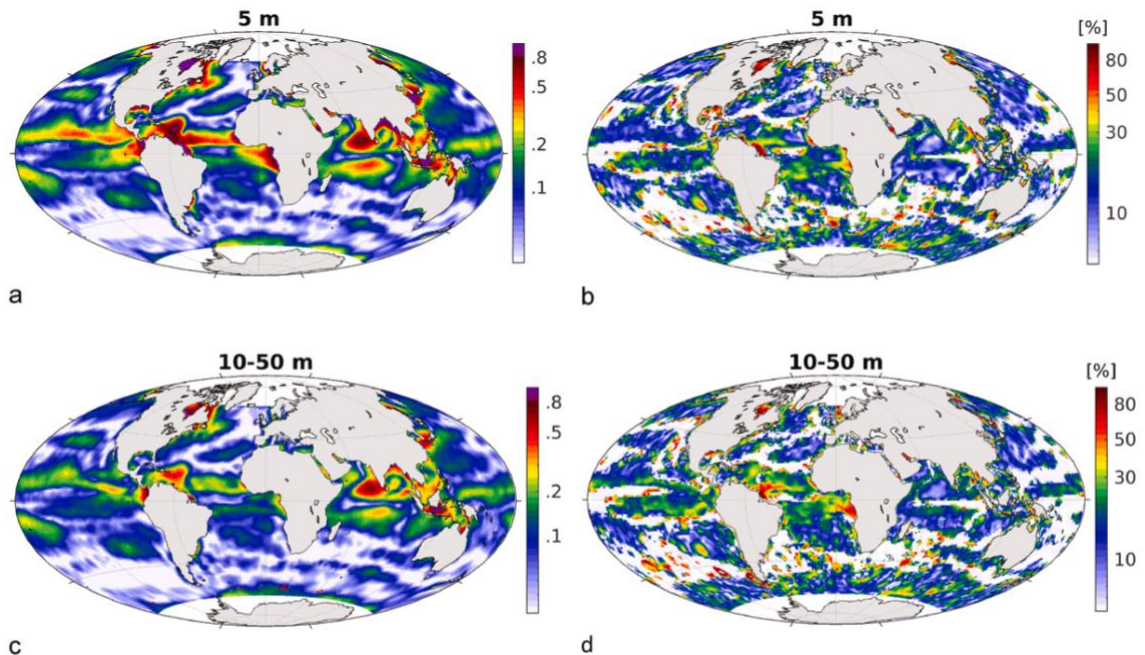


Figure 6-2 Ensemble-mean annual amplitude in salinity variability of the ensemble in situ data, at (a) 5 m depth and (c) in the layer averaged from 5 to 50 m. Ensemble spread of the annual amplitude in percent relative to the total amplitude at (b) 5 m depth (d) and 50 m depth layer.

Measuring and validate salinity in near-coastal and highly dynamic regions remains problematic. In the case of satellite data uncertainty is enhanced and in contrast, more accurate in situ data remain too sparse in near-coastal regions due to various reasons, such as lack of Argo sampling there, but also the negative influence of enhanced ocean pollution on salinity data quality (Wong et al., 2018). In these regions, the community has to improve their ability of making use of enhanced availability of satellite products to interpolate the sparse set of in situ data. An enhanced salinity annual cycle can be found in the surface layer (5 m depth) in regions of enhanced surface forcing, e.g., under ITCZs in the Pacific and Atlantic, in front of large rivers, but also in other regions with large coastal freshwater input. In contrast, in the 5 to 50 m range associated with dynamically driven features the salinity seasonal cycle reaches deeper, e.g., in the Arabian Sea affected there by seasonal changes in circulation. However, the percentage spread within the in situ data ensemble confirms that in either depth range the amplitude of the salinity seasonal cycle is not easy to estimate from the existing in situ database (see Figure 6-2). This holds especially within the tropics, where the disagreement between in situ data is around 30%, locally up to 50%. In contrast, a good agreement can be seen in the low variability subtropical salinity maximum regions.

As for other observables and un-observable quantities, much hope has to be therefore placed also on salinity information inferred through ocean reanalysis products. With respect to the seasonal cycle, existing reanalysis products show the same amplitude patterns as in the in situ ensemble mean, however, with weaker amplitudes at both depth ranges. Finally, satellite SSS annual amplitude shows the best results, from which much finer spatial structures can be revealed than from the in situ and reanalysis products. This holds especially in frontal regions. In

addition, substantially higher amplitudes of the seasonal cycle can be revealed in the river outlet regions and under the tropical ITCZs. It remains to be seen to what extent high-resolution data assimilation efforts that make use of satellite SSS fields will build on this advantage, will make a better link to changes in surface forcing but also expand the information of salinity variability to greater depths than can be inferred from satellite data alone.

This study shows the importance of measuring salinity, especially, sea surface salinity to get a better picture of variability and trend patterns. The satellite retrieved sea surface salinity data are of importance for climate studies, and help analyzing variations from small-scale/high-frequency to lower-frequency signals. With the version 3 of the CCI+SSS data product we have now approximately 11 years of satellite SSS data, providing a first description of interannual variability patterns and, in combination with the longer in situ salinity timeseries, potentially yielding a first insight into decadal variabilities.

6.2 Summary Salinity Science Seminar

A CCI-SSS Salinity Science Seminar took place on 26-27 September 2019 at the Institute of Oceanography of Universität Hamburg (Germany). The seminar was organized by a DFG-funded German national effort of freshwater and salinity changes in the Atlantic, chaired by the Institute of Oceanography, and with support from LOCEAN i.e., the seminar was a joint seminar of the German Project FOR1740 and the CCI+SSS consortium. More than 30 scientists from research institutes from Europe and USA attended the Workshop presenting current research on ocean salinity.

The focus of the meeting was put on actual research and brought together recent expertise of data assimilation and salinity processes based on models and ocean salinity observations as well as validation studies and feedback regarding the new CCI+SSS product.

The objectives were addressed during the two days starting with the opening of the meeting by the host (Detlef Stammer), meeting objectives from ESA (Craig Donlon) and from CCI+SSS perspective (Jacqueline Boutin) followed by an overview of the user requirements regarding satellite SSS data and a presentation of the first CCI+SSS product. Using the new CCI+SSS data set salinity gradients in the tropical Atlantic were analysed, as well as the driving processes behind the seasonal variations of river plumes in the Gulf of Guinea. Furthermore, model and observational salinity variability were compared, and underlying processes analysed. A detailed study of validation results regarding the new CCI+SSS data set was presented and showed the high quality of SSS data. In this context, caveats were discussed with the user group and a list was completed, which is finally included in the data set metadata.

6.3 Scientific Studies

6.3.1 CASE STUDY 3: Water cycle in the Bay of Bengal

By Jérôme Vialard (LOCEAN)

Monsoon rain and rivers bring large freshwater input to the Northern Bay of Bengal (BoB), yielding low Sea Surface Salinity (SSS) after the monsoon. The resulting sharp upper-ocean salinity stratification is thought to influence tropical cyclones intensity and biological productivity by inhibiting vertical mixing. Despite recent progress, the density of in situ data is far from sufficient to monitor the BoB SSS variability, even at the seasonal timescale. The advent of satellite remotely sensed SSS (SMOS, Aquarius, SMAP) offers a unique opportunity to provide synoptic maps of the BoB SSS every ~ 8 days. Previous SMOS SSS retrievals did not perform well in the BoB. We showed that improved systematic error corrections and quality control procedures yield a much better performance of the new “debiased v4” CATDS level-3 SSS from SMOS (~ 0.8 correlation, 0.04 bias and 0.64 root-mean-square difference to more than 28,000 collocated in situ data points over 2010–2019). The SMOS product now performs equivalently to Aquarius and is slightly inferior to SMAP over the BoB. In particular, SMAP and SMOS are able to capture salinity variations close to the east coast of India ($r > 0.8$ within 75–150 km of the coast). They thus capture the seasonal freshening there, associated with equatorward advection of the Northern BoB low-salinity water by the East Indian Coastal Current (EICC) after the summer monsoon. Being confident that the product captures SSS variations in the BoB well, we studied interannual SSS variability in that basin from the 10 available years of data, which is strongest in boreal fall in relation with the Indian Ocean Dipole (IOD), a mode of indigenous climate variability of the Indian Ocean, while having a weak relation with El Niño in the neighbouring Pacific Ocean. The East Indian Coastal Current normally transports freshwater from rain and rivers in the Northern BoB southward along the coast of India after the monsoon, creating a narrow freshwater tongue nicknamed the “river in the sea” (e.g., Chaitanya et al. 2014; Akhil et al. 2014). During positive IOD events, the EICC weakens under the influence of the equatorial remote forcing.

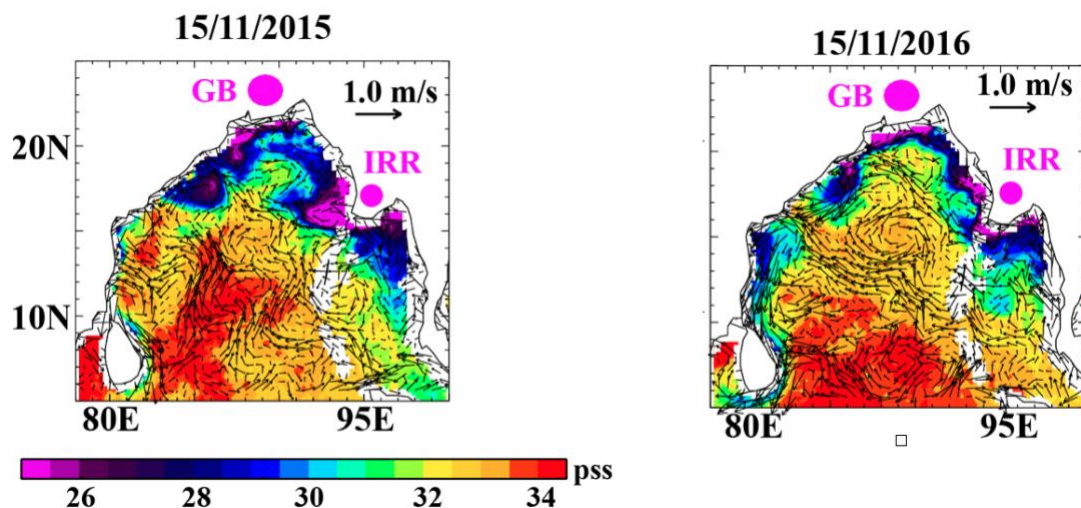


Figure 6-3: Bay of Bengal SSS from the CCI product in November 2015 (left) and 2016 (right). With very strong salinity contrasts due to large freshwater inputs and an energetic circulation, the Bay of Bengal is a good laboratory to monitor large salinity signals. Here, the very fresh waters associated with the Irrawaddy and Ganges-Brahmaputra estuaries are strongly influenced by mesoscale eddies and the interannual variability. The opposite polarities of the “Indian Ocean Dipole” climate mode in 2015 (IOD+) and 2016 (IOD-) result in a clear southward East Indian Coastal Current in 2016, and the Ganges-Brahmaputra freshwater plume extends further southward along the India coast that year



This reduces the southward export of freshwater along the coast of India and leads to a dipole with fresh anomalies in the Northern and salty anomalies in the South-western BoB. This confirms results from earlier studies based on modelling, sparse in situ data, or shorter satellite records, but this time from a 10-year long SSS record. Overall, our study indicates that the new SMOS retrieval can be confidently used to monitor the BoB SSS and to study its mechanisms. The very good performance over the BoB of the CCI+SSS multi-satellite product developed by the European Space Agency merging SMOS, Aquarius and SMAP data can be seen from Figure 6-3. Figure 6-3 shows the Bay of Bengal CCI+SSS in November 2015 and November 2016. Very strong salinity contrasts due to large freshwater inputs can be observed. Furthermore, an energetic circulation can be seen from the ocean current data overlaid. Here, the very fresh waters associated with the Irrawady and Ganges-Brahmaputra estuaries are strongly influenced by mesoscale eddies and the interannual variability. The opposite polarities of the “Indian Ocean Dipole” climate mode in 2015 and 2016 result in a clear southward East Indian Coastal Current in 2016, and the Ganges-Brahmaputra freshwater plume extends further southward along the India coast that year.

Validation (see PVIR) of CCI+SSS indicates that CCI+SSS product is likely to be the best alternative to describe and understand the BoB SSS variability in future studies. As this dataset becomes longer, it will allow an increasingly accurate description of the BoB SSS interannual variability. Comparison of the CCI+SSS v3 with v1 shows, that relative to the v1 product, the v3 product has applied a less stringent flagging to pixels that are near land surfaces. In the Bay of Bengal, this mostly benefits the spatial coverage near the Ganges-Brahma estuary, in the north of the Basin, and near the Andaman and Nicobar Islands, to the southeast. Comparing the two datasets to the same in situ data sample indicates that the v3 product is generally equivalent or slightly improved relative to the v1 product over most regions, except in the Northern Bay of Bengal. Further information can be found in the PVIR.

One of the important science questions to resolve using this new dataset is: what is the dominant mode of SSS year-to-year variability in the Bay of Bengal and the corresponding processes. Previous studies using sparse in situ data (Chaitanya et al. 2014), modelling (Akhil et al. 2016b) or shorter satellite remote sensing datasets (Fournier et al. 2017; Akhil et al. 2020) did indicate that the leading mode of interannual variability of SSS in the Bay of Bengal was associated to a modulation of the EICC variability by the Indian Ocean Dipole, a mode of climate variability in the Indian Ocean.

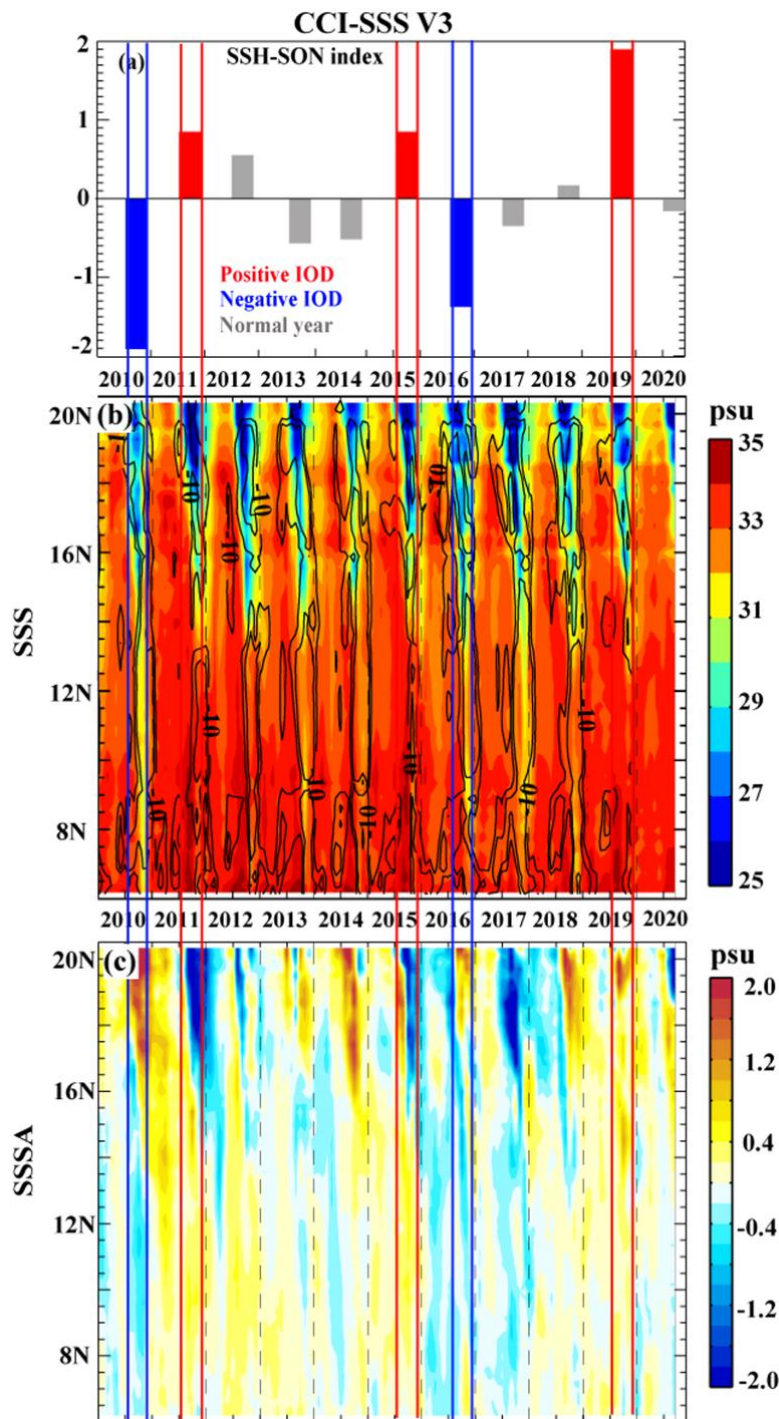


Figure 6-4 2010-2020 time series for a) the average September-November value of the DMI (Dipole Mode Index, and index of the IOD) with positive events marked in red and negative ones in blue; b) SSS within 100 km of the east coast of India (Southward EICC occurrences are marked by the black contours) and c) as b but for SSS anomalies with respect to the 2010-2020 mean seasonal cycle.

The v3 dataset allows to examine the influence of a large positive IOD event in 2019 on SSS along the east coast of India (Figure 6-3). As for previous occurrences in 2011 and 2016, the IOD+ event of 2019 was associated with positive SSS anomalies along the east coast of India, i.e., less

freshwater advection from the northern BoB in relation to an abnormally weak southward EICC. Negative SSS anomalies along the coast of India symmetrically occurred during the two IOD-events of 2009 and 2016. The v3 dataset however raises several interesting questions:

- Some years that are not associated with clear dipole events do display coherent SSS anomalies along the coast of India, as e.g., 2014 or 2017. What are the physical processes that cause these anomalies? Can those anomalies be related to known oceanic signals in the Bay of Bengal, such as eddies or the oceanic dynamical response to atmospheric intraseasonal variability?
- There are also large interannual anomalies in the Northern BoB, sometimes in phase opposition with the signals described above, sometimes not. The model analysis of Akhil et al. (2016b) suggests that those more local anomalies near estuaries are related to interannual variability of the river runoffs, rather than to changes in ocean currents. Preliminary analyses suggest that the current dataset is still too short to clearly conclude about that.

6.3.2 Tropical Instability Waves in the Atlantic Ocean: investigating the relative role of sea surface salinity and temperature from 2010 to 2018

By Lea Olivier et al. (see Olivier et al. 2020)

Tropical instability waves (TIWs) in the equatorial Atlantic Ocean are analysed during a 9-year period 2010-2018 using satellite derived sea surface salinity observations, sea surface temperature (SST), sea level anomaly and Argo profiles. In particular, the weekly 50-km SSS time series from the Climate Change Initiative project provides an unprecedented opportunity to observe the salinity structure at a scale closer to the TIW SST scale.

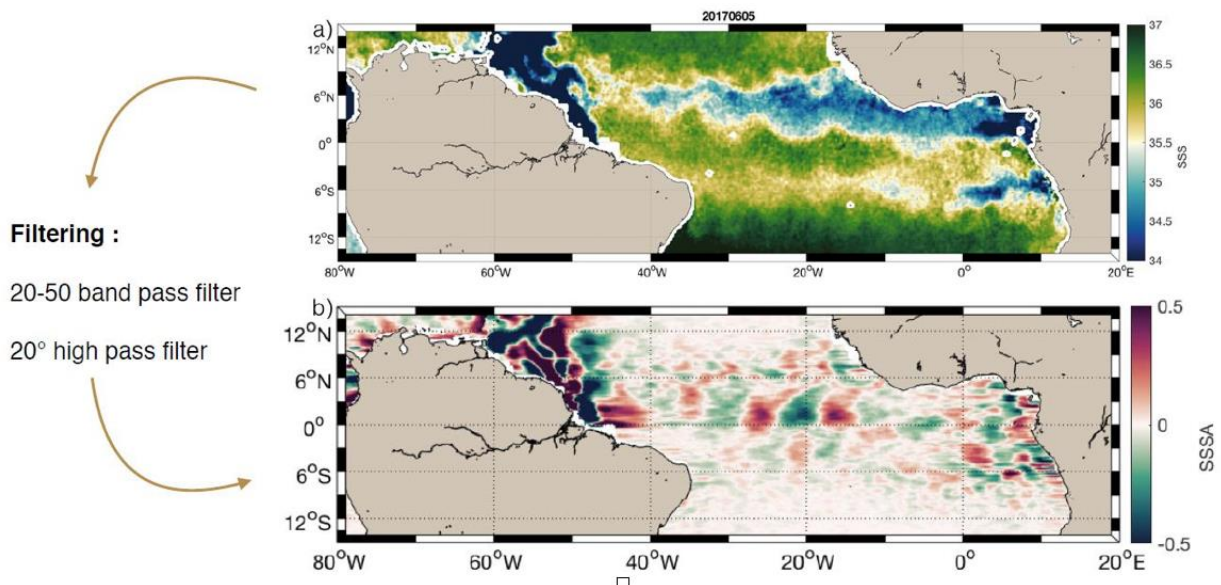


Figure 6-5: Snapshot of SSS (upper panel) on the 5th of June 2017 showing the deformation of the SSS front at 1°N by tropical instability waves. (Lower panel) Snapshot of band pass filtered SSS data (20-50 day band pass filter, 20° longitude high pass filter)

Presented in Figure 6-5 is a snapshot of SSS and band pass filtered SSS (SSS anomalies, SSSA) for 5th June 2017 showing the deformation of the SSS front at 1°N by tropical instability waves. The temporal evolution of SSSA, SST and SLA along 1°N is presented in **Error! Reference source not found.** from Jan-2010 to Dec-2018, showing the propagation of TIWs each year from May-September in all datasets.

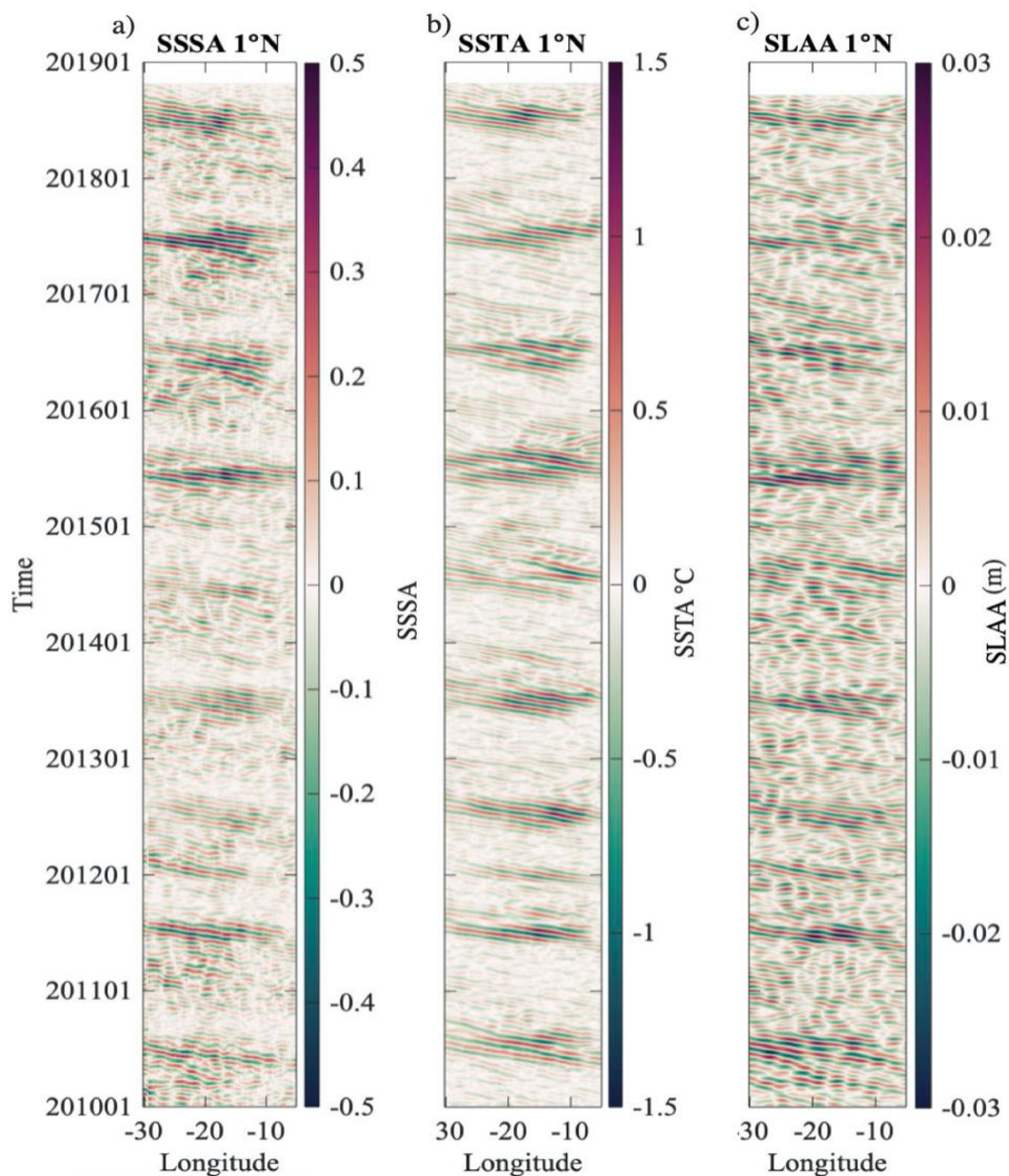


Figure 6-6: Hovmöller diagram of the sea surface salinity anomalies (SSSA, left), SST (middle) and sea level anomaly (SLA, right) at 1°N over the period January 2010 to December 2018.

From here it can be seen that westward propagation along 1°N is found on all data sets, when filtered to retain the 20-50 days periods and 0°-20° wavelengths to highlight the TIWs. At this latitude, the mean 2010-2018 westward propagation speed is 0.4 m/s. It has been previously shown that TIWs in the Atlantic are particularly intense at 1°N (Chelton et al., 2000; Lee et al., 2014) and it is also the case in the data used for this study. Between 2010 and 2018, we observe the presence of TIWs at 1°N every year in SST, SSS and sea level anomaly. We examine the relative contributions of SSS and SST to the horizontal surface density gradient on seasonal and interannual time scales and how they contribute to the TIW properties and energetics. Argo profiles are used to investigate the associated subsurface signals. Figure 6-7 presents a snapshot of the SSS, SST, density and chlorophyll on the 5th of June 2017 showing also the clear deformation of the SSS and density front at 1°N.

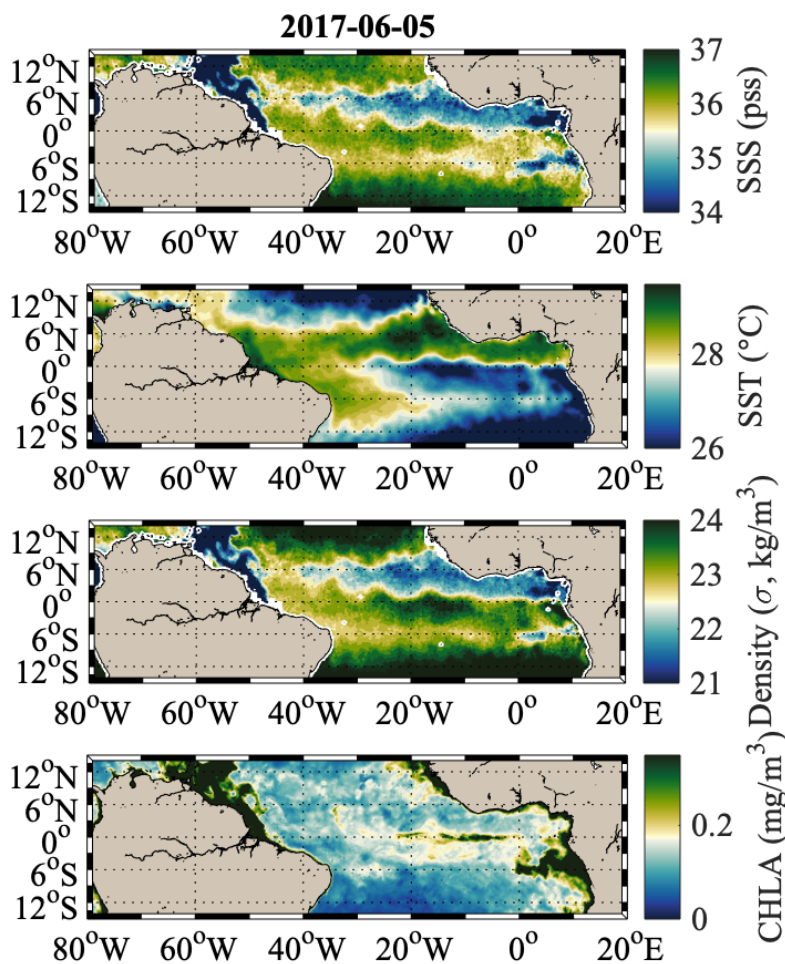


Figure 6-7 5th June 2017 snapshot of a) sea surface salinity, b) sea surface temperature, c) sea surface density (σ =density-1000 kg/m³), d) surface chlorophyll.

For the central Atlantic TIWs, the maximum of the SST contribution to the density anomaly lags the SSS contribution by approximately one month. Argo vertical profiles indicate that temperature and salinity both significantly contribute to TIW-related density anomalies. In the top 60 m of the water column, salinity and temperature contribute in almost equal proportions



to the perturbation potential energy (PPE). Our study shows that even on a very well documented phenomenon such as the TIWs, the earlier lack of salinity observations was an issue impeding its full understanding. Not retaining salinity in the computation of PPE would underestimate the PPE by almost a factor 2. This implies that when trying to estimate the respective barotropic and baroclinic energy sources for the TIWs, not taking into account salinity would result in underestimating the baroclinic contribution. There is a large interannual variability modulating the seasonal signal, with different variations in SSS, SST and SLA. The Atlantic Meridional and zonal modes contribute to understand these variations for some specific years, such as in 2015, but hardly explain the totality of the interannual variability. Therefore, this 9-year long satellite SSS time series emphasizes the importance of having a long-term time series of satellite salinity. To remove the uncertainty concerning the role of the dominant modes in the interannual variability, a much longer time series (20 to 40 years) is needed. Moreover, the Argo coverage over 9 years is large enough to study the TIWs seasonality, but the analysis is still limited due to uncertainties. It is also too sparse to investigate in detail the interannual variability. Having access to the subsurface structure of TIWs significantly improves the understanding of the seasonal cycle. It also shows that the surface signal can be different from the subsurface one, underlining the complementarity between surface satellite and subsurface in situ data. It would therefore be very enriching to investigate the interannual signal in the same way, for example also including PIRATA mooring data. Furthermore, the SSS satellite product has a one-week temporal resolution. Improving this resolution could lower the smoothing of the wave in the product and better resolve the high frequency variability.

6.3.3 A fresh plume in the northwestern tropical Atlantic during the EUREC4A- OA/ATOMIC program in February 2020

By G. Reverdin et al. (see Reverdin et al. 2021)

In early February 2020, a freshwater plume was extensively documented by satellite and in situ observations spreading over the North Atlantic near the Demerara Rise (7°N/54-56°W). It was initially surface trapped with stratification up to 10-m depth and a width on the order of 120 km. Its freshwater content corresponded to 2 to 3 meters of Amazon water and was distributed down to 40 m, though most of it was in the top 20 m. The first transects on February 2 (not shown) indicate an inhomogeneous structure with a propagating front in its midst on the shelf. Minimum salinities of close to 30 pss were observed close to the shelf break on February 5th. The salinity minimum eroded in time but was still found on in situ and satellite observations to have minimum values on the order of 33.3 pss 13 to 16 days after it spread off the shelf break, and 400 km away. At this time, the mixed layer had not deepened to more than 20 m as evidenced by ocean velocity data from a saildrone transect. The off-shelf flow lasted for roughly 10 days, contributing to a plume area extending over 100000 km² and likely associated with a freshwater transport on the order of $0.15 \cdot 10^6$ m³/s. The off-shelf plume was steered by eddies up to 12°N and extended westward toward the Caribbean Sea. Its occurrence seems to be the result of 3 days of favourable wind direction closer to the Amazon estuary, which contributed to northwestward freshwater transport along the shelf to the area where it separated. The presence of such events of

freshwater transport in February is documented since 2010 in 7 out of 10 years, and in 6 of those years including 2020, they are preceded by a change in wind direction between the Amazon estuary and the Guyanas that is favourable to northwestward freshwater transport toward the shelf break.

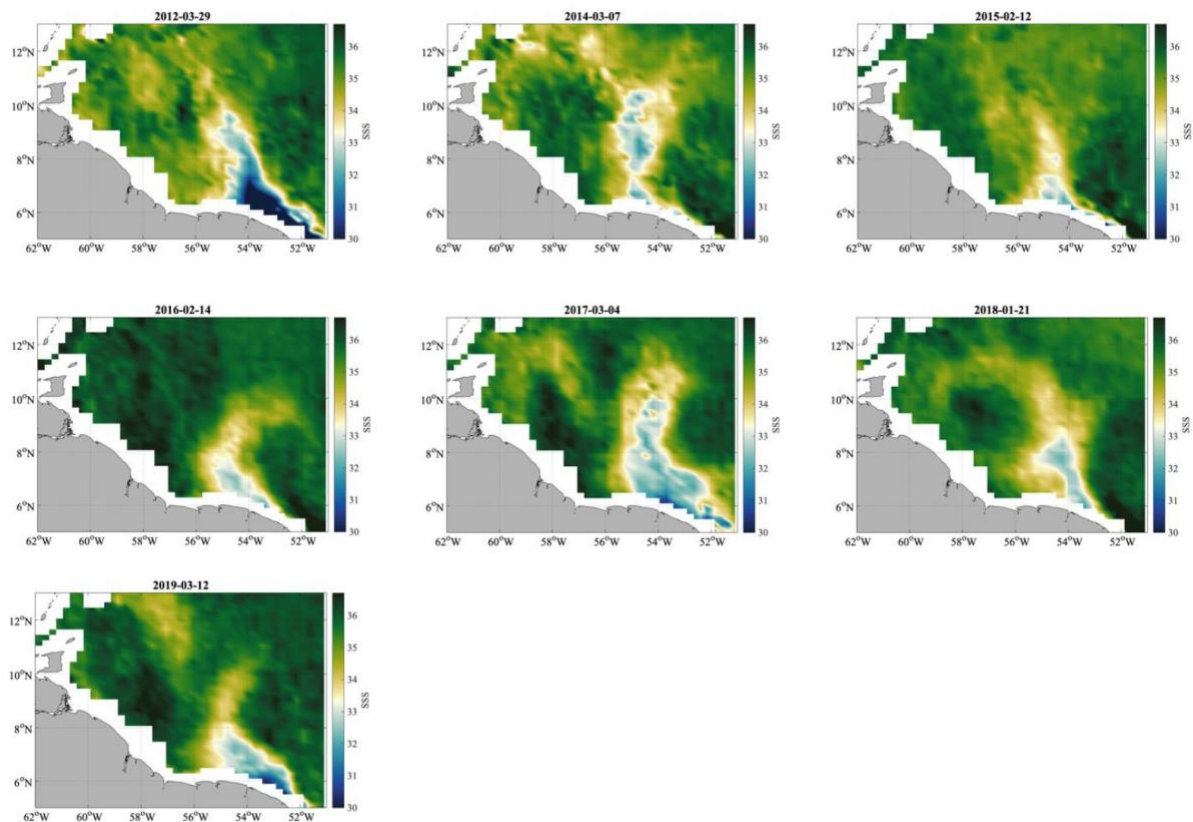


Figure 6-8: CCI+SSS daily snapshots of a fresh plume in the northwestern tropical Atlantic from 2012 to 2019.

In Figure 6-8 weekly SSS for all occurrences of fresh plumes extending at least to 10°N and east of 56°W in January-March 2010-2019 (note that 2010, 2011 and 2013 don't have events) are shown. The weekly SSS fields are generated by the Climate Change Initiative Sea Surface Salinity (CCI+SSS) project (v2.31, doi:10.5285/4ce685bff631459fb2a30faa699f3fc5). For each event, the week retained corresponds to peak extension of the fresh plume. Notice that most of these plumes suggest the presence of an anticyclone to its east.

6.3.4 CASE STUDY 2: Climate variability reconstruction in the Atlantic

By Juliette Mignot, Gilles Reverdin, Eric Guilyardi and Victor Estella-Perez (LOCEAN).

An attempt is being performed to reconstruct the climate system over the 20th century at IPSL. Such reconstructions are useful to gain understanding on the mechanisms shaping the climate variations over this period. Furthermore, they may be used for initial conditions of decadal prediction systems. Recent studies have shown that initializing a decadal prediction system with



initial conditions coming from the same climate model maximizes the prediction skill, in particular over the Pacific (Liu et al. 2016) and Atlantic (Yeager and Robson 2017).

Our approach to perform such reconstructions is to combine our climate model together with observations. Given the uncertainty in the subsurface oceanic observations and our objective to avoid jeopardizing the physical equilibrium in the ocean interior, we favour constraints only on the ocean surface.

Previous work has shown that nudging the climate simulation only towards observed SST anomalies yields interesting skill in terms of reconstructing the past climate variations and predicting the future climate (Ray et al. 2015; Swingedouw et al. 2013; Mignot et al. 2016). Nevertheless, perfect model studies have also suggested that adding information from sea surface salinity significantly increases the quality of the reconstruction (Servonnat et al. 2014; Ortega et al. 2017, Estella-Perez et al, in rev.). The lack of global surface salinity data set at the horizontal resolution of the climate models (1°) and covering climatic periods (of the order of the last 50 years) has prevented us up to now from applying this methodology to historical conditions.

Here, we explore the possibility of using sea surface salinity data provided by the CCI+SSS project to reconstruct climate variability at decadal timescales using climate models. More precisely, we propose to address questions about the characteristics of the SSS provided to perform such reconstructions: resolution and accuracy. For this we used a coupled model to nudge a control simulation using SST and SSS from a target period to reconstruct the variability of this period. Given the primary role of the Atlantic Meridional Overturning circulation (AMOC) for climate decadal variability in the coupled models, the quality of the reconstructions will be assessed from correlation of the magnitude of this circulation with the targeted one. Firstly, we consider a Target period of 100 years from a pre-industrial run of the IPSL-CM5A2 (Sepulchre et al., in revision) from which we use the SST and SSS to nudge three different control periods. The three simulations would be represented as an ensemble depicted by their mean and their standard deviation. Within this framework, we modify initially the regions of assimilated SSS and SST to understand the impact of these in our reconstructions.

Secondly, we focus on the impact of uncertainty of the assimilated data, as the product provided by the CCI+SSS project has an associated uncertainty and error. We aim to put a superior limit to the error up to which we can still use satellite data in our climate reconstructions. On the one hand, we test the sensitivity of different regions to our reconstructions by perturbing the SSS adding a white noise in certain locations. On the other hand, we aim to find a way to include the explicit uncertainty of the CCI product as one of the input information in our reconstructions. For example, the more uncertain an observation of SST and SSS is, the weaker our restoring could / should be. Also, since uncertainty changes with space and time, we could explore the implications of this variability. The use of more advanced assimilation techniques, such as ensemble Kalman filter (e.g., Counillon et al. 2016), including by construction information on the data uncertainty, is also under study.

In our initial tests, we limited the region to which SST and SSS were assimilated. We considered three initial tests: 1) global SST and global SSS (Glob-Full) restoring, 2) SST and SSS restricted within both hemispheres (45°N-45°S) and 3) limited to within ±60° in both hemispheres and extending to extra latitudes in the North Atlantic up to 70° (60NSPG-60S). The reconstruction of the AMOC, measured as maximum of the overturning circulation at 48°N (Figure 6-9), shows a higher correlation with Target for the two configurations including higher latitudes, Glob-Full and 60NSPG-60S. Assimilating data only up to 45°N in both hemispheres does not provide a good reconstruction of the large-scale oceanic reconstruction in the Atlantic and thus presumably of the large-scale low-frequency climate variability in general. In the Atlantic, between 45° and 70° latitudes we have the main regions of deep-water formation in the North Atlantic, which explains the improvement on performance when these latitudes are considered. We can conclude that including this range, 45°-70°N, is crucial to reconstruct correctly the AMOC in the North Atlantic.

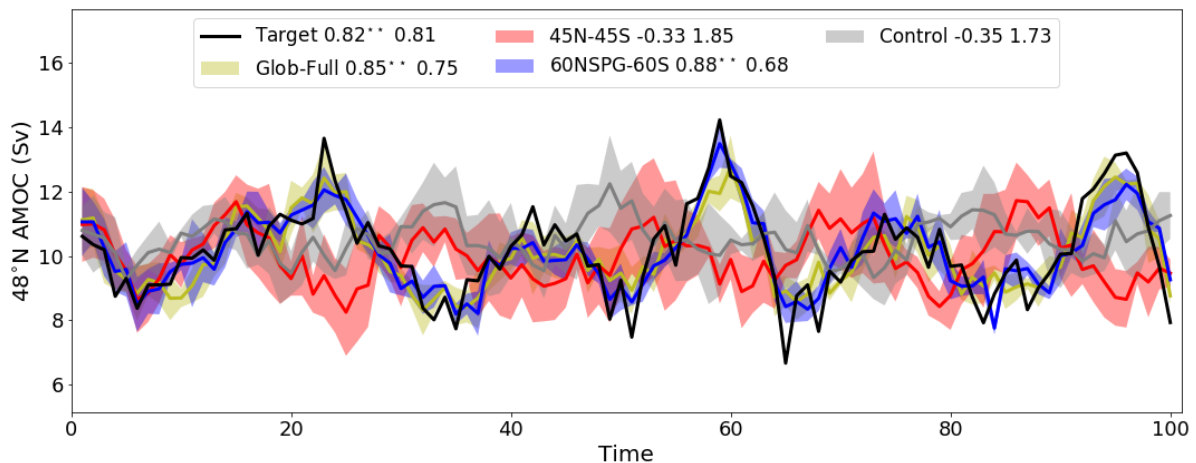


Figure 6-9 Evolution of the AMOC at 48° N for global SST and global SSS (Glob-Full in yellow), limited to 45° in both hemispheres (45N-45S in red), limited to 60° in both hemispheres (60NSPG-60S in blue) and control runs (Control in grey). Numbers in the labels indicate correlation and root mean square error of each experiment with the Target over the 100 years. 99 % confidence level of correlation is indicated as **.

To understand the impact of uncertainty, we run a first perturbation test starting from the benchmark simulation, Glob-Full (considering global SSS and SST): At each model grid point (latitude and longitude) at each time step, the monthly initial target file was perturbed by adding a random value from a spatial white noise of mean 0 and standard deviation 0.2:

$$SSS_{target}^{WN0.2}(lat, lon, t) = SSS_{target}(lat, lon, t) + WN(0, 0.2)$$

We then used this modified salinity to nudge our model.

The results on the AMOC reconstruction (Figure 6-10) present large anomalies with respect to Glob-Full in the AMOC reconstruction for the WN0.2psu ensemble. The error is 2.79 Sv on average over the 100-year period, almost double the standard deviation of our target. Despite this, we can still maintain the variability of the Target, as the oscillations of about 20 years are still present in both experiments. This result shows that accuracy of our reconstruction is very limited by the error of the data on a global scale. We still have to understand if this sensitivity is

global or local to certain regions. Uncertainty in CCI+SSS L4 data is not uniformly distributed. It has a spatial distribution and values changing accordingly. Next steps will consist in 1) using a pattern and values like the available L4 uncertainty to the target file and test the impact of such uncertainty on our reconstructions and 2) pinpointing the key regions/periods to be monitored for AMOC and on which future improvements of CCI+SSS should focus.

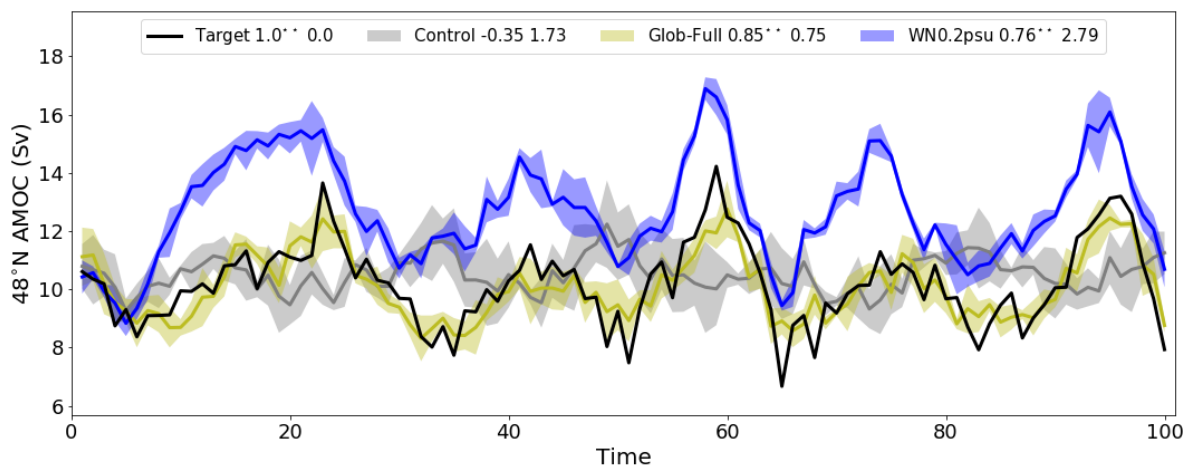


Figure 6-10: Evolution of the AMOC at 48°N for global SST and global SSS (Glob-Full in yellow), perturbed with a white noise 0.2 (WN0.2psu in blue) and control ensemble (Control in grey). Numbers in the labels indicate correlation and root mean square error of each experiment with the Target over the 100 years. 99 % confidence level of correlation is indicated as **.

The knowledge gained in a perfect model framework will be later transferred to actual historical reconstructions. We already have performed historical reconstructions using the binned data described in Friedman et al. (2017) following the protocol developed in Estella-Perez et al. (in review). We have not yet included the impact of uncertainty, but with the work here developed, we will be able to deliver climate reconstructions of the 20th century accounting for observation uncertainty. This will allow us to study the SSS (SST) signatures reconstructing climate/atmosphere inter-annual modes of variability (typically ENSO, Atlantic Nino/equatorial mode, NAO, EAO...), as well as Atlantic dipole and Caribbean signals when going to the decadal frequency domain.

6.3.5 CASE STUDY 4: Salinity stratification and small-scale variability

By N.Reul, N. Kolodziejczyk, O. Houdegnonto, C. Maes and T. O’Kane (LOPS)

Among the different physical processes contributing to the present climate changes and their impact on the ocean productivity and marine ecosystems, little attention has been paid to the large-scale contributions of stratification changes within the water column. Stratification, which is associated with the density difference between the surface and the deeper layers, characterizes the stability of the water column, and therefore influences the potential for vertical exchange of properties such as, heat, momentum, nutrients, or dissolved oxygen. Due to the lack



of in situ observations the salinity effect on stratification has often been neglected as compared to its thermal counterpart. Consequently, the differential effect resulting from the atmospheric forcing in terms of the temperature and salinity variability remains mainly unexplored. Rather than focusing on the classical halocline vs. thermocline definitions, the present study proposes to consider the respective thermal and saline dependencies in the Brunt-Vaisala frequency (N^2) in order to isolate the specific role of salinity stratification in the layers including the main permanent pycnocline. The role of salinity is differentiated through its stabilizing or destabilizing effect on stratification along the water column, and the specific role of the SSS field is addressed.

Combined with in situ profile of salinity and temperature, the new CCI+SSS data allow to refine our knowledge of the co-variability between SSS, Barrier Layer thickness (BLT), as well as subsurface thermohaline properties (e.g., density stratification) in various regions of the tropical oceans. Geographical distribution and temporal variability of BL properties inferred from satellite SSS have been demonstrated along the western tropical Pacific warm pool SSS front (Qu et al., 2014), western tropical Atlantic (Moon et al., 2014, Reul et al., 2014c), and Indian ocean (Felton et al., 2014; Moon et al., 2014; Sengupta et al., 2016, Köhler et al., 2018). The established regional surface-to-subsurface relationships can be used to infer maps of subsurface properties from satellite SSS, such as BLT (Felton et al., 2014), mixed layer depth (Schlundt et al., 2014; Köhler et al., 2018), as well as haline and thermal stratification parameters (Schiller and Oke, 2015; Su et al., 2015; Chen et al., 2017; Reul et al., 2014c).

To investigate the capability of the satellite CCI+SSS estimates to help monitor the horizontal distribution of the vertical density stratification over the large tropical river plume waters, we first looked if the SSS and/or SST values in the large tropical river plume waters can be used as proxies for the strength of the vertical stratification below the plumes and surrounding waters as first determined from ARGO floats.

Estimates of upper ocean thermohaline conditions are derived from ARGO profile data. At each ARGO float cast, the vertical salinity $S(z)$ and temperature $T(z)$ vertical profile fields are used to determine the SSS, SST, density profile $\rho(z)$, Mixed Layer Depth (D_σ), salinity ($S = S(z = D_\sigma - 5m)$) and temperature ($T = T(z = D_\sigma - 5m)$) at a depth 5 m below the MLD, as well as the maximum of the squared Brunt-Väisälä frequency found in the upper 200 m of the ocean. The MLD definition follows De Boyer Montégut et al. (2004, 2007).

A match-up database of co-located data between CCI-SSS and ARGO floats, and derived surface and subsurface parameters has been built. The co-localized SSS (from either ARGO or CCI-SSS) and SST were binned averaged as a function of the maximum (along the vertical) buoyancy frequency at co-located ARGO/CCI-SSS points with bins of width 2.5 cycles per hour (cph). We used the preliminary CCI-L4-ESA-MERGED-OI-V1.5-MONTHLY satellite SSS products for illustration (covering the period 2010-2018). The results for four different large tropical river plume regions are analysed:

- Region 1: Mississippi River plume [98°W- 81°W;24°N-31°N]
- Region2: Amazon & Orinoco River plumes [78°W-25°W;5°N-30°N]

- Region 3: Congo River plume: [0°-13°E; 10°S- 0°S]
- Region 4: Bay of Bengal [79°E-98°E;9°N 22°N]

An example is provided in Figure 6-11 for the case of the Amazon and Orinoco River plumes.

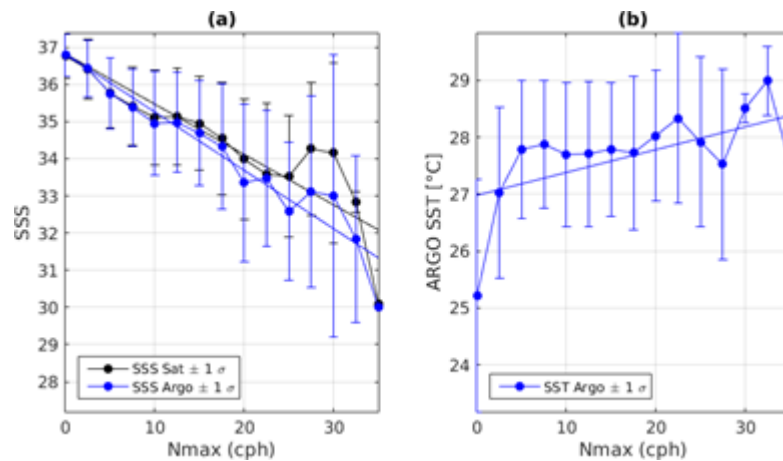


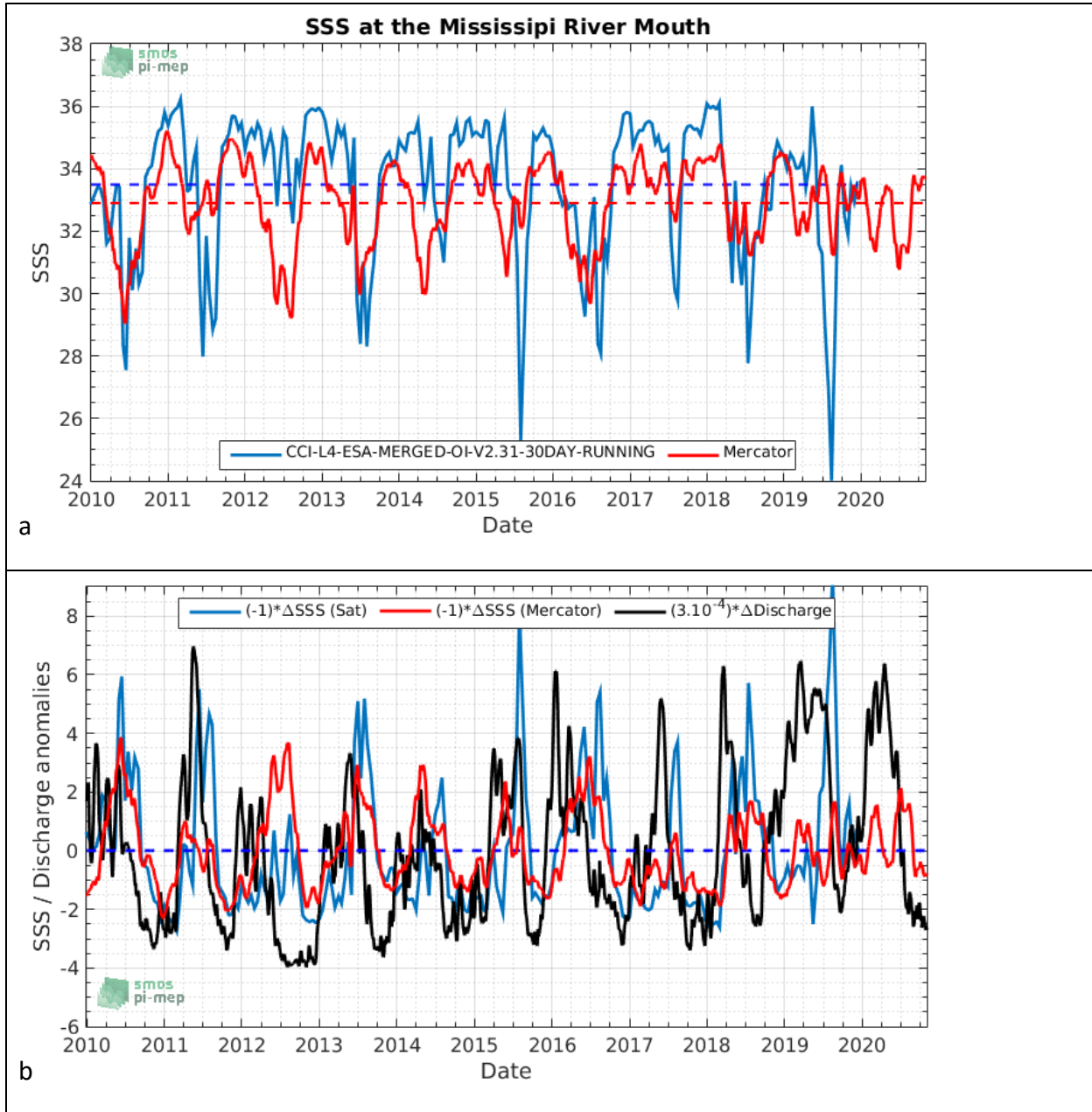
Figure 6-11: Averaged relationships between (a) SSS, (b) SST, and the maximum buoyancy frequency N_{max} determined below the surface from ARGO floats within the Amazon and Orinoco river plume extent ([78°W-25°W; 5°S-30°N]) over 2010-2018. Linear fits are indicated by black and blue solid lines. The average values of SSS and SST are given by the dotted lines per N_{max} value bins of width 2.5 cph.

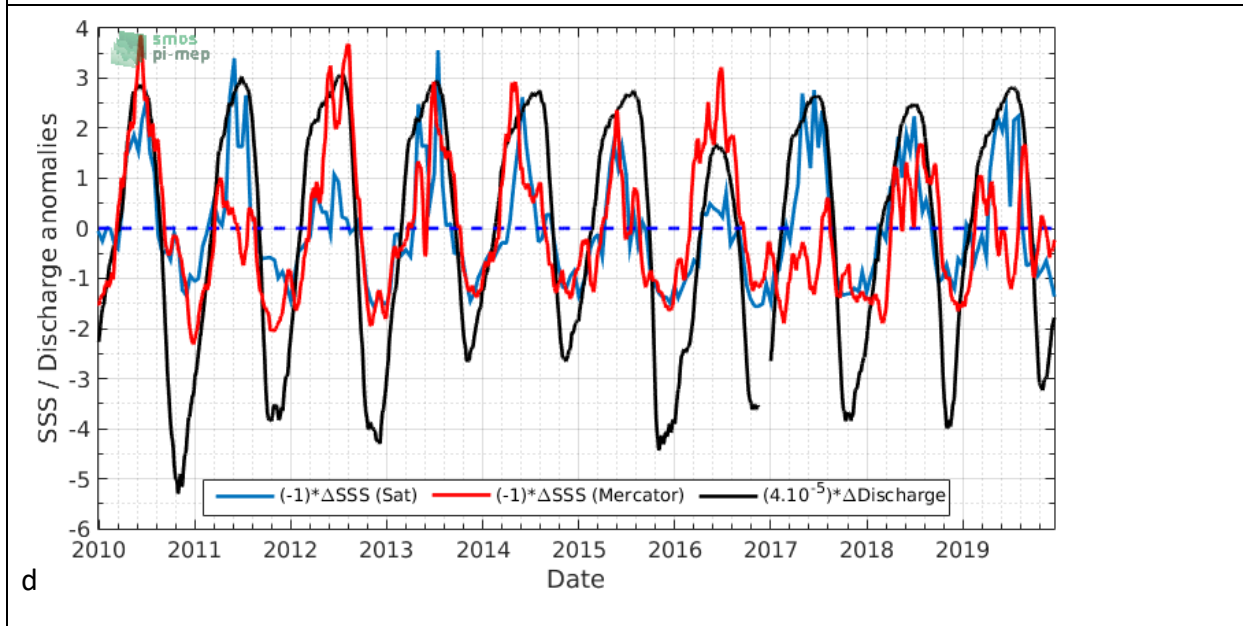
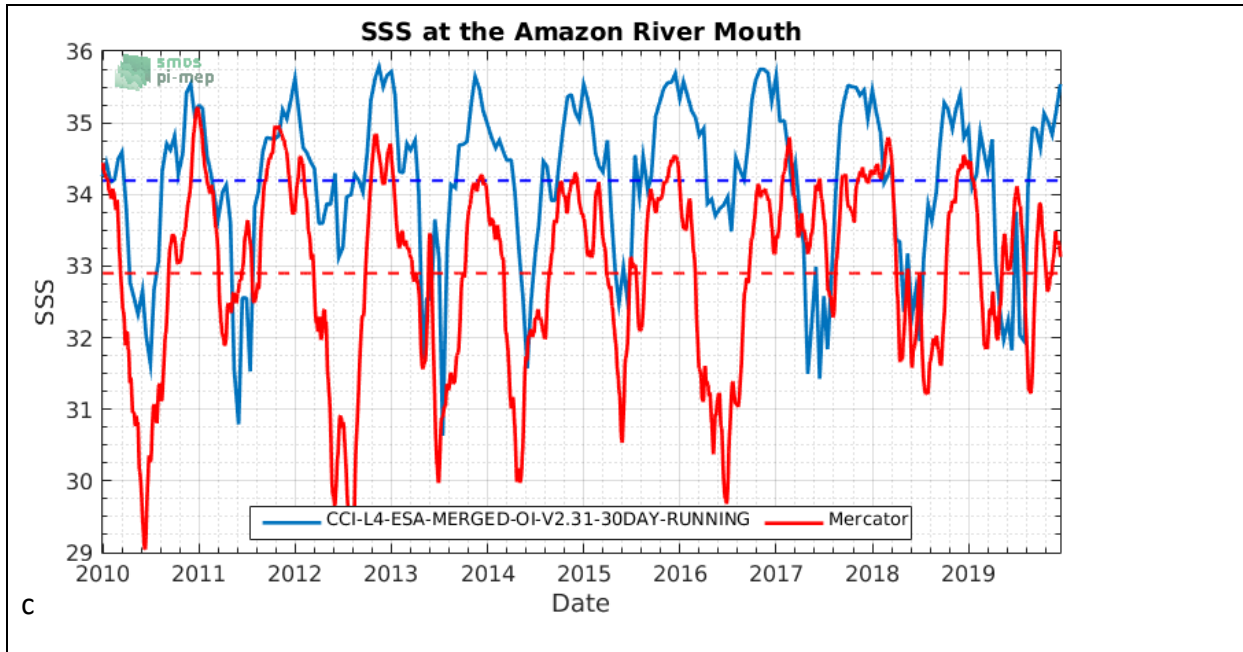
Quasi-linear ‘mean’ dependencies between SSS and N_{max} similar to the one observed in Figure 6-12 for the case of the Amazon/Orinoco river plume are found for all the 4 above regions. The slope is however changing from one river plume to the next. Definitely, the quasi-linear empirical laws between SSS and N_{max} can be used in reverse to map the vertical stratification (N_{max}) from the CCI-SSS time series. The strength of the salt stratification in these regions and its interannual variability will depend on the amount of river discharge, the strength of the advection/mixing by ocean, and atmospheric circulations as well as the input of freshwater by local rain. We also look at the combination of CCI+SSS and SST data to refine the N_{max} estimates.

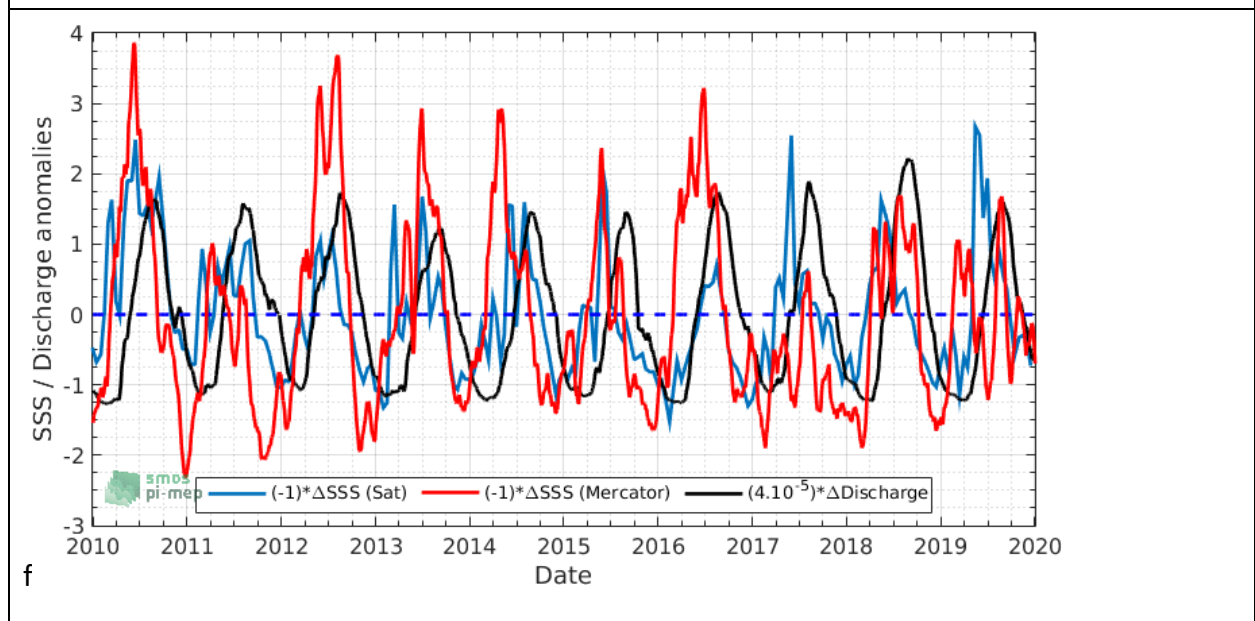
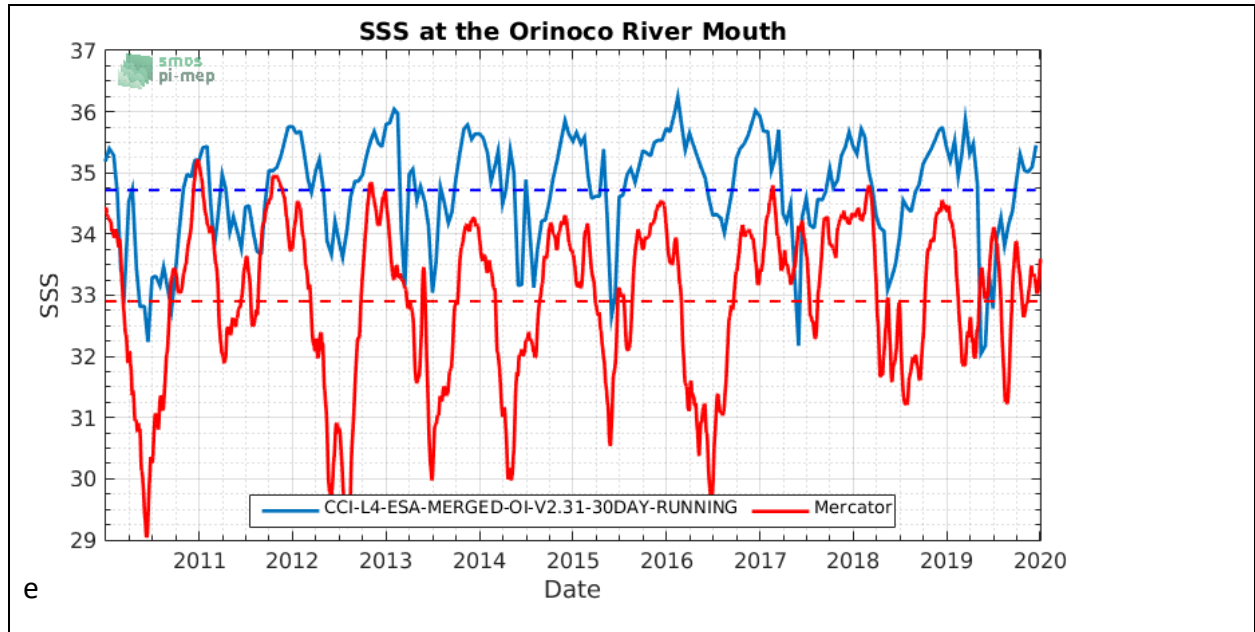
As a first step towards analysing the climate variability in the upper ocean vertical stratification N_{max} of these 4 regions indirectly from CCI+SSS, the correlation between SSS and river discharge has been already analysed and compared to CMEMS model SSS forecasts. As found, there are significant differences between the CMEMS model SSS and CCI SSS at the mouth of the major rivers.

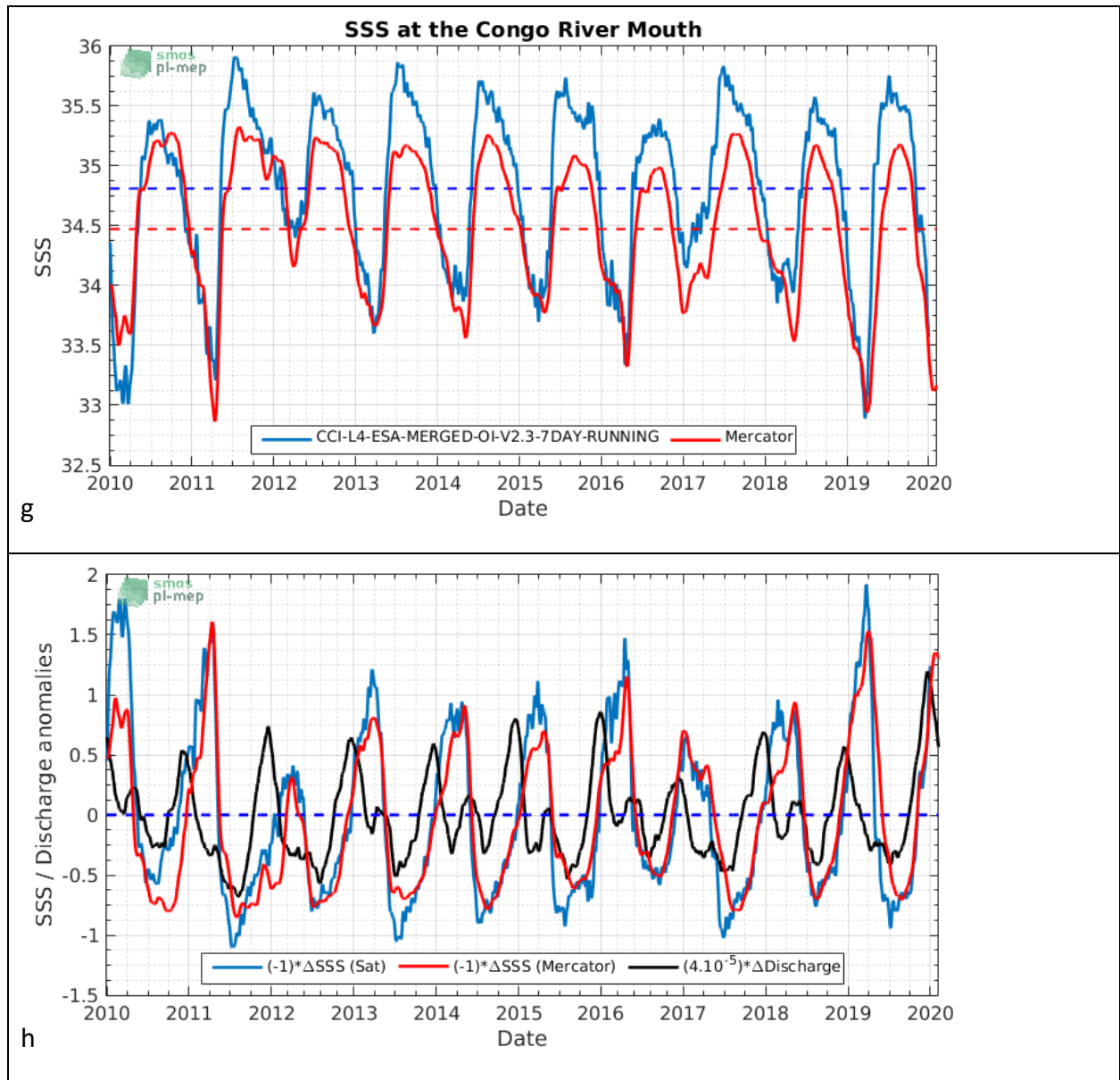
As illustrated in Figure 6-16 Figure 6-12 the interannual variability in SSS at the river mouth and its correlation with river discharge can now be studied. The ESA Pilot Mission Exploitation Platform (Pi-MEP) for example provides access to a large ensemble of in situ and satellite datasets allowing systematic comparisons between available datasets, also in river plume regions. We will study specific years with strong SSS anomalies in terms of co-variability with large scale climate indexes (ENSO, IOD, etc.) as well as with ocean circulation and atmospheric variability. Trends over the decade between maxima/minima of discharge and maxima/minima of SSS anomalies at

the river mouths will be analysed to provide insights into the land to ocean freshwater fluxes and evolution over these major river plumes.









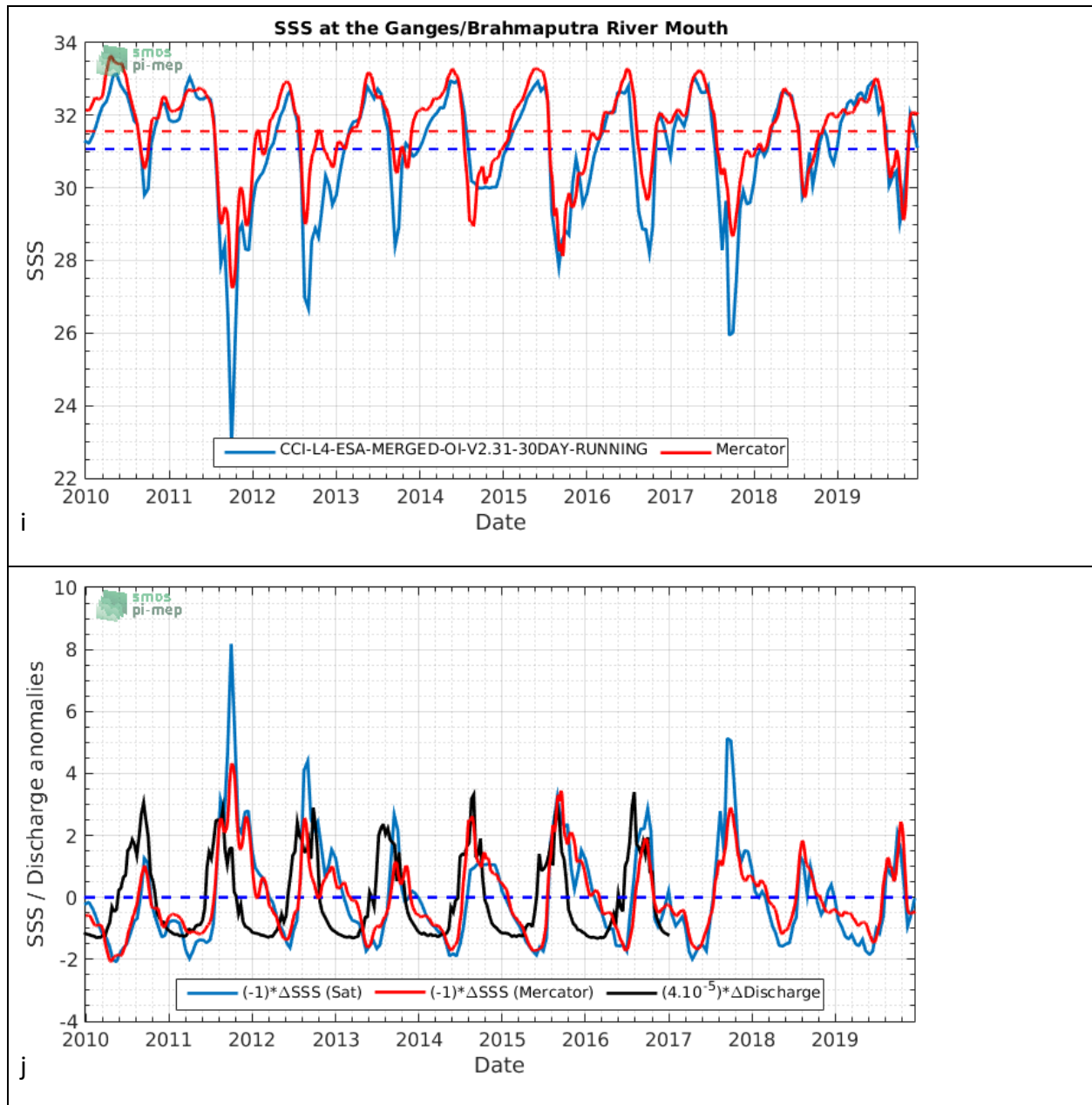


Figure 6-12 (a ,c, e,g, i) Time series of CCI (blue) and CMEMS-Mercator model (red) SSS spatially averaged at the mouth of 4 major tropical river plumes (a: Mississippi River Mouth, c: Amazon River Mouth, e: Orinoco River Mouth, g: Congo River Mouth and i: Ganges/Brahmaputra River Mouth). b,d,f,h,j,: Time series of CCI (blue) and CMEMS (red) model SSS and river discharge (black) scaled anomalies (obtained by subtracting the record mean value from individual value). Scale factors are indicated in the legend.

Small scales, stratification and river plume in the Gulf of Guinea

Nicolas Kolodziejczyk (Nicolas.Kolodziejczyk@univ-brest.fr), LOPS, IUEM, Brest, France

Odilon HOUNDEGNONTO (odilon.houndegnonto@univ-brest.fr), LOPS, IUEM, Brest, France



Assessing SSS Mesoscale features in CCI-SSS v2.31 and v3.2 products

The surface mixed layer thermohaline structures at meso-scale to submesoscale (smaller than the local radius of deformation, *Chelton et al.*, 1998) are ubiquitous features in the global ocean. They contribute to horizontal and vertical heat and salt exchange and vertical re-stratification (*Fox-Kemper et al.*, 2005). They have a global impact on ocean circulation and climate since they contribute to the cascade of energy from large scale toward the smallest scales of diffusive mixing (*Callies and Ferrari*, 2013). Eventually, they have a major impact on biogeochemistry and ecosystems. The submesoscale processes are characterized by very intense vertical velocities that allow strong exchanges of carbon, oxygen and nutrient between surface and subsurface ocean (*Lévy and Martin*, 2013).

Until early 2010, satellite capabilities for observing surface thermohaline variability have been mainly relied on the observation of Sea Surface Temperature (SST) only, resolving small scale features such as 10 km (*Kilpatrick et al.*, 2015). In contrast, synoptic image of Sea Surface Salinity (SSS) was not available and *in situ* SSS at high resolution are only available from few high-resolution sections from Thermosalinograph (TSG) survey from ship of opportunity repeated transects or cruise campaign (*Kolodziejczyk et al.*, 2015b). Since 2010, thanks to ESA SMOS mission, then NASA Aquarius and SMAP missions, 4-7 days global maps of SSS at resolution between 40-100 km are now available permitting observation of larger mesoscale features in subtropical and tropical region (*Reul et al.*, 2014; *Kolodziejczyk et al.*, 2015a).

To check the effective capability of the new CCI-SSS product v2.31 and v3.2 (7 day) to monitor the large mesoscale features of SSS in the subtropical and tropical regions, the CCI product's SSS were systematically co-localized and compared with TSG SSS along existing repeated transect in Subtropical North Atlantic and Tropical Atlantic. An effective metric to assess the SSS horizontal variance and scale content of both products is to compute the spectra and coherency spectra between TSG SSS and CCI-SSSv2.31 and v3.2 (*Boutin et al.*, 2018)

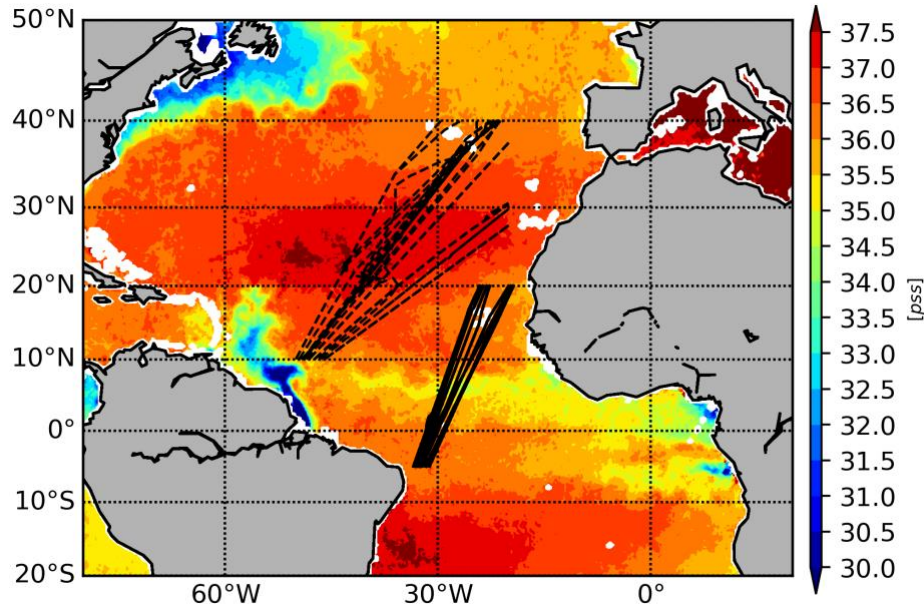


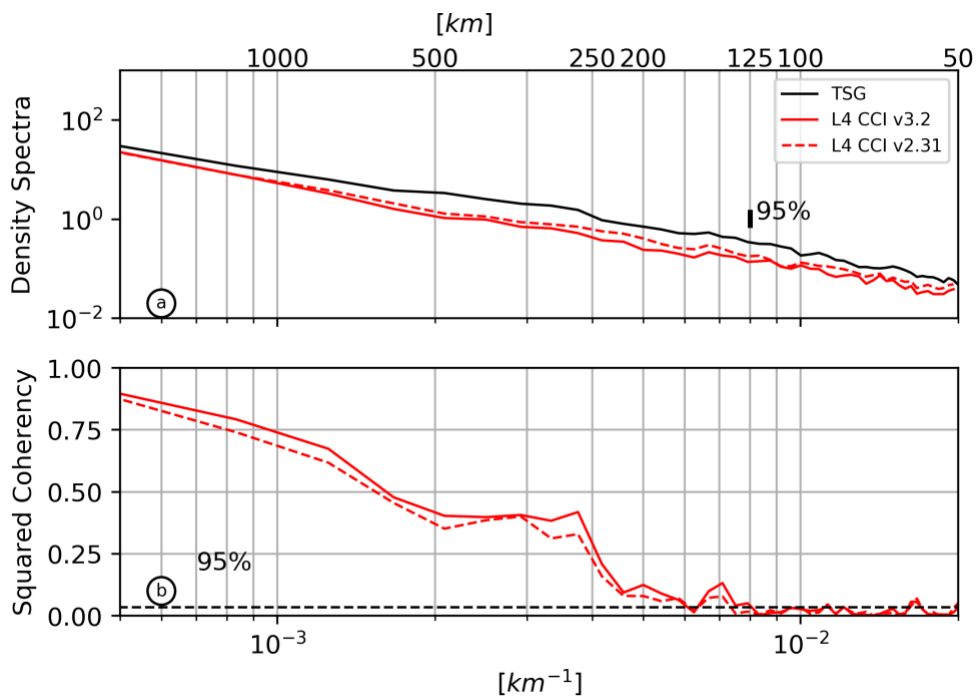
Figure 6-13 CCI+SSS on 30 June 2011 with 93 TSG transects in the Subtropical North Atlantic (dashed) and 26 TSG transect in the Tropical Atlantic (solid lines).

SSS TSG transects were collected from ships of opportunity (representative of salinity at 10 m depth), resolving horizontal SSS features around 2-3 km (Alory *et al.*, 2015). Two regions were chosen for the present study (Figure 6-13): i) the North Atlantic subtropical SSS maximum (50-20°W/10-40°N), where 88 transects between 2011-2016 are available; and ii) the Tropical Atlantic (40-10°W/5°S-20°N) where 26 transects between 2014-2016 are available. Individual transects were visually inspected and suspicious transects were discarded. To reduce uncertainty due to noisy individual spectrum from each individual transect, spectra were averaged for both regions.

The horizontal SSS coherency spectra refers to the coherency of the SSS horizontal variability between the co-located TSG SSS and CCI+SSS products, *i.e.*, the level of correlation of the SSS signal for a given wavelength range. This allows to assess the actual capability of CCI+SSS products to observe mesoscale features (>50 km) from the noise and spurious SSS contamination.

In the Subtropical North Atlantic (Figure 6-14a), in spite of slightly less energy between 50-1000 km wavelength, CCI+SSSv2.31 and v3.2 horizontal variance spectrum, both TSG and CCI+SSS spectra show good agreement, *i.e.*, comparable slopes between 50-1000 km are observed. This suggests that for this range of wavelength the variance of mesoscale features is probably smoothed in CCI+SSS products. The CCI+SSSv2.31 spectra exhibits however slightly more energy than the CCI+SSSv3.2 spectra. Interestingly, the coherency spectra (Fig.-14b) exhibit quasi-linear decrease from large scale (coherency>0.75 for wavelength > 1000 km) to mesoscale (coherency~0.30 for wavelength ~ 300 km). The significance at 95% is lost for wavelength below

200 km. This suggests that wavelength smaller than 300 km are poorly represented in the CCI+SSS product. The CCI+SSSv2.31 spectra exhibits however slightly less coherency than the CCI+SSSv3.2 spectra, likely due to slightly more noised SSS v2.31 fields. Overall, this is consistent with previous study on investigating the SMOS LOCEAN CEC L3 product (*Boutin et al., 2018*) in the same region, however with a slightly better coherency for CCI+SSS product. And no significant differences from the previous PVIR-CCI+SSS report are reported.



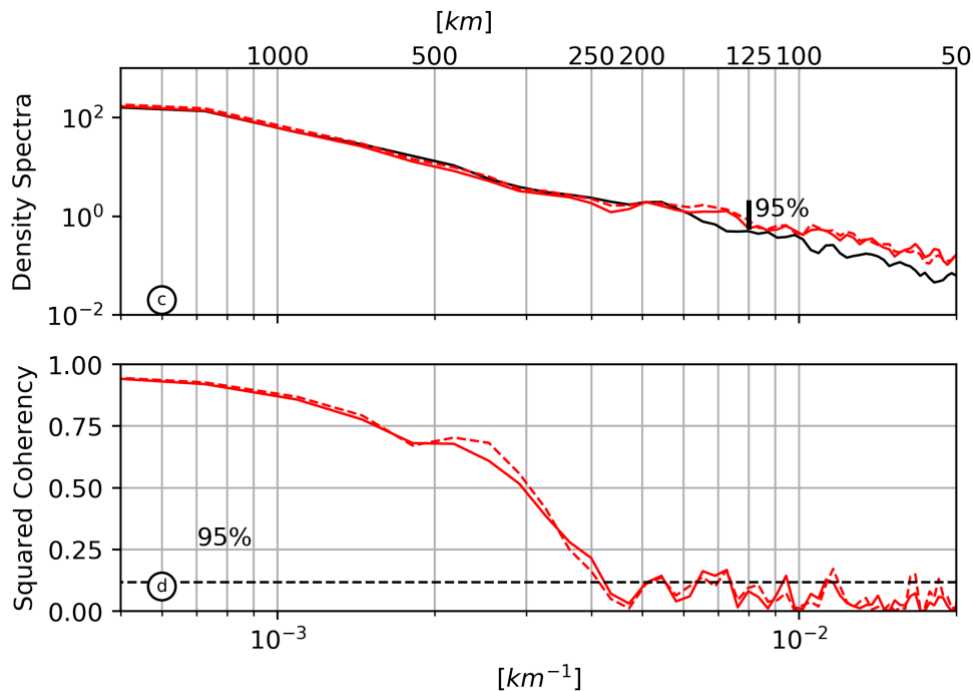


Figure 6-14 a) Density spectra from 88 co-located TSG (black); CCI+SSS v2.31 (dashed red); CCI+SSS v3.1 (solid red) SSS transects in Subtropical North Atlantic. Vertical thick black bar is the level of confidence at 95%. b) Coherency between the TSG and CCI+SSS SSS transects. Dashed line is the level of significance at 95%. c) Density spectra from from 26 colocated TSG(black)/CCI+SSS(red) SSS transects in Tropical Atlantic. Vertical thick black bar is the level of confidence at 95%. d) Coherency between the TSG and CCI+SSS SSS transects. Dashed line is the level of significance at 95%.

In the Tropical Atlantic (Figure 6-14c), TSG and CCI+SSS spectra show very comparable behaviors, the level of variance and slope have comparable values. Furthermore, both spectra also show a relatively high level of coherence (Figure 6-14d) at wavelength larger than 300 km (coherency>0.5). In the Tropical Atlantic region, the coherency drops off observed at wavelength smaller than 250 km suggests that the CCI+SSS product is not able to consistently resolve scale smaller than 125 km. This is slightly better than the CCI+SSS v1 products reported in the previous PVIR report. No significant differences are reported between CCI+SSS v3.2 and v2.31.

In conclusion, in the subtropical Atlantic, the CCI+SSSv2.31 and v3.2 product can resolve wavelength of the order of 300 km. This wavelength corresponds to horizontal mesoscale features of the order of about 150 km (gradient, eddy). However, the level of coherency between TSG SSS horizontal variability and CCI+SSS drops rapidly at mesoscale. In the tropics the level of coherency remains high up to 300 km wavelength, then drops dramatically.

The loss of coherency at smaller horizontal wavelength could be explained by i) the limiting resolution of SSS satellite mission (>50 km), ii) remaining noise and artifacts in the CCI+SSS data, and iii) smoothing from objective analysis procedure of the CCI+SSS products. Nevertheless, it is worth pointing that inconsistency between instantaneous and point-wise measurements from the TSG data and co-localized CCI+SSS products (7 days, 50 km) may be responsible for shift and



lag between TSG SSS measurements and CCI+SSS products SSS along transects, resulting in loss of coherency for the smaller and faster SSS mesoscale structures.

Comparison of SSS-CCI v2.31 product in Congo Plume

Gulf of Guinea is a key region for the regional climate variability. A noticeable regional climate feature is the Western African Monsoon, which is strongly influenced by sea surface temperature and subsurface conditions in the Gulf of Guinea, including stratification, mixing and circulation. Large river runoff has strong impacts on the near surface thermohaline stratification and mixing in the Gulf of Guinea. In return, the river plume extensions are strongly influenced by seasonal and interannual wind driven surface circulation. In the eastern Gulf of Guinea, historical *in situ* dataset suffers from sparse sampling providing few information on the river plume variability (*Da-Allada et al., 2012*). On the other hand, few model study have focus on the Eastern Gulf of Guinea SSS dynamics (*Camara et al., 2016*). SSS satellite missions offer a new opportunity, to investigate the eastern Gulf of Guinea river plume dynamics. Furthermore, the recent enhancement of database in the Gulf of Guinea (Argo, TSG, CTD casts) provides new perspective to investigate the stratification and small-scale vertical structure within river plumes of the region (*Houdengnonto et al., 2021*).

A first step is to validate the CCI+SSS products in the Eastern Gulf of Guinea (GG). In the Gulf of Guinea (15°S-10°N/10°W-15°E), the available *in situ* SSS observations in the upper 5-10 m depth (TSG, Argo, CTD casts) have been co-located with CCI+SSSv2.31 products (Figure 6-15a,b). Scatter plots for TSG and Argo/CTD products reveal a very good agreement with an insignificant bias (~ 0.01 pss), and a RMSD of 0.46 for the comparison with TSG data and 0.36 for the comparison with the Argo and CTD data. This difference can be explained by the larger spread of the *in situ*/CCI+SSSv2.31 products near coast (Figure 6-15). Note that, the statistics in the GG are slightly less good (RMSD: ~ -0.02) than for the collocation of the SSS+CCIv1 reported in the previous PVIR report. Indeed, TSG measurements are generally carried out closer to the coast where residual coastal bias and RFI contamination can increase the noise in the satellite measurement.

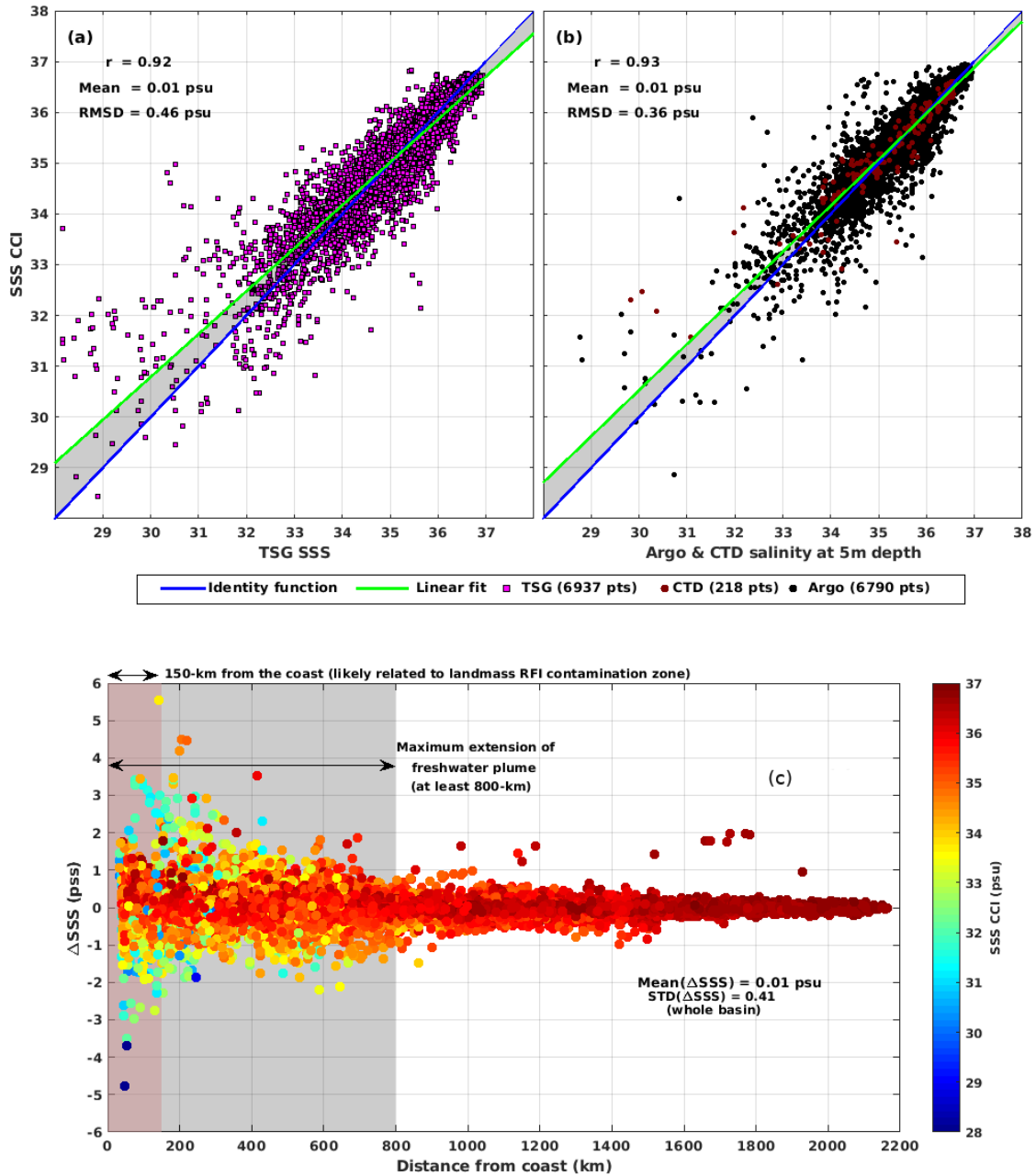


Figure 6-15: Scatter plot of TSG SSS measurements (a) and Argo/CTD data (b) with the CCI+SSS v2.31 products in the Gulf of Guinea (15°S-10°N/10°W-15°E) over the period 2010-2019. (c) distribution of the difference of co-located *in situ*/CCI+SSSv2 (in pss) as a function of the distance from the coast.

Moreover, near coast the river plume signal generates strong SSS horizontal gradients and shallow surface salinity stratification, thus it implies larger difference when discrepancy between *in situ* observation and satellite products.

6.3.6 CASE STUDY 5: Comparing salinity variability between observations and models

By Detlef Stammer, Julia Köhler, Meike Sena Martins, Armin Köhl (UHAM)

We aim to investigate the quality of the new CCI+SSS ECV product through a comparison of the satellite retrieved salinity variability with other in situ and model information both spatially and temporally. Available for such a comparison is a collection of in situ data which include all in situ data available. Also available is the access to climate coupled models (e.g., NCAR). All available data sets are used together to investigate the salinity variability of the Atlantic, but also the Indian and the Pacific Ocean.

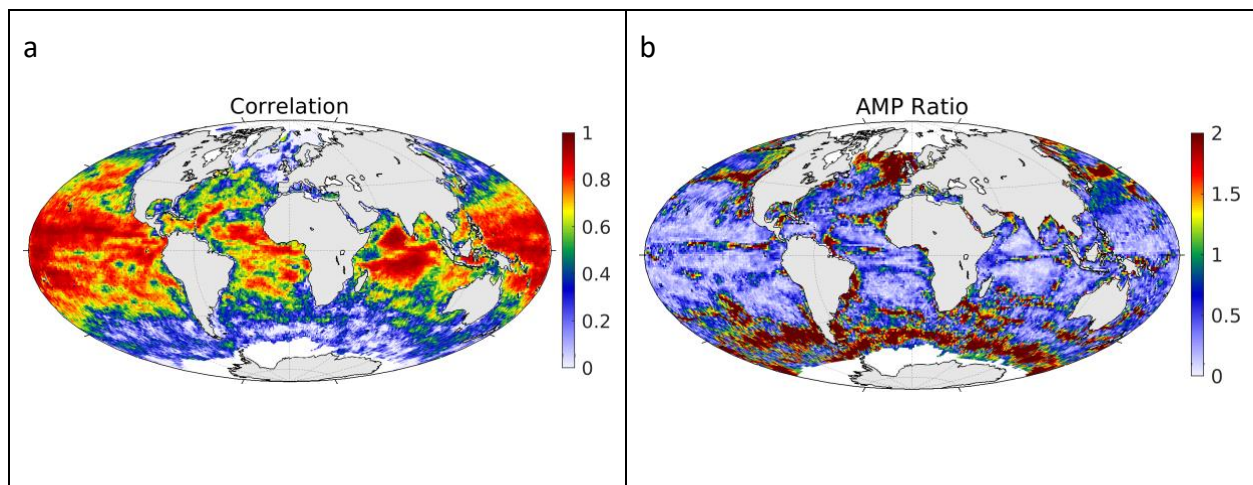


Figure 6-16: (a) Correlation of satellite CCI+SSS v3.2 and uppermost ENS salinity. (b) Ratio of the annual amplitude of the difference between satellite CCI+SSS v3.2 and ENS uppermost salinity and the annual amplitude of the ENS uppermost salinity. (from Stammer et al., 2020)

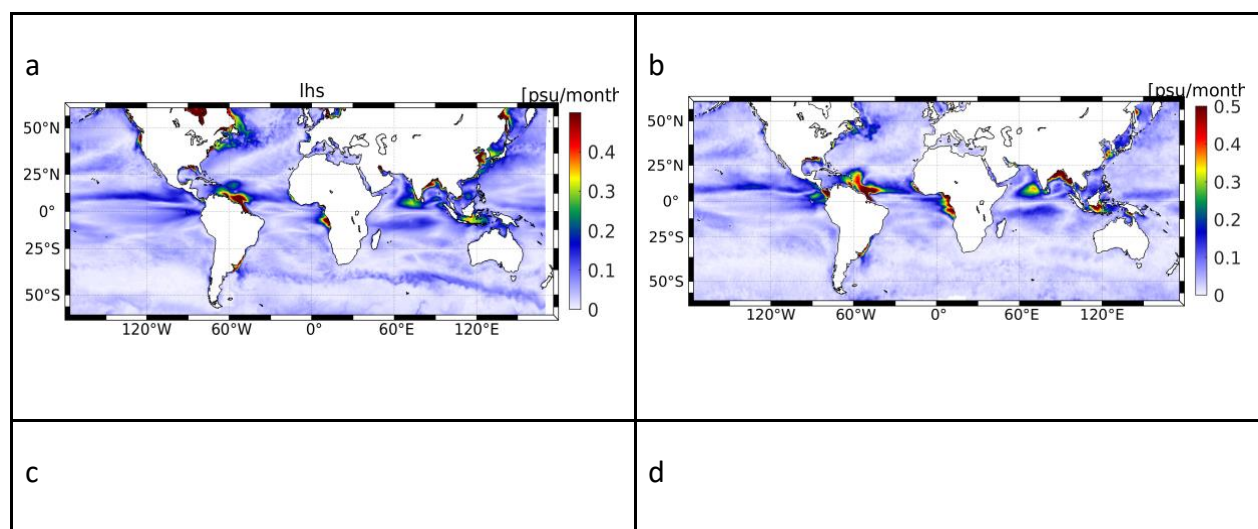
To look further into the similarities and differences between the in situ and satellite salinity fields, presented in Figure 6-16, Figure 6-16a is the correlation of the CCI+SSS and in situ uppermost salinity (an in situ ensemble product including all in situ data available: WOA18, EN4.2, SIO, IPRC, JAMSTEC and ISAS_15, in the following named ENS) over the 2011–2017 period, reaching values larger than 0.8 in the tropical and subtropical regions of all oceans. The correlation is low in the Amazon outflow region, in the western Arabian Sea, and in subpolar and polar regions.

Many factors can contribute to the low correlation observed in these areas, like low SSS and uppermost salinity variance, measurement errors in the satellite SSS (e.g., land contamination and RFI, challenging retrievals in cold waters) and representative errors in the in situ fields. Heavy rain events and salinity stratification in the upper layers can also cause low correlations, which could be of importance in the river outlet regions like the Amazon outflow. Studies by Köhler et al. (2018), Wilson and Riser (2016), Akhil et al. (2014), highlight the importance of vertical stratification, e.g., in the northern Bay of Bengal. This is confirmed by the ratio of the annual amplitude of the difference between satellite CCI+SSS and ensemble in situ uppermost salinity and the annual amplitude of the in situ uppermost salinity, shown in Figure 6-16b: values >1 indicate that the annual cycle of the differences is larger than the annual salinity cycle. This holds especially in the high latitudes, subtropical regions and in a small band at the equator and could be an indicator of enhanced salinity stratification there, but also of enhanced data errors. We also note that many of the regions with ratios above one are also regions with a small

amplitude of the seasonal cycle suggesting that the seasonal component is not well-defined and may be affected by the impact of small-scale processes. All in all, the validation results, described in more detail in the PVIR document, show that the higher temporal and spatial resolution of the satellite data leads to a more comprehensive impression of small-scale high-frequency variability than the in-situ data does. Hereafter, mixed layer salinity budgets were calculated to identify the driving processes of salinity variability on various timescales. On the one hand, they were based on in situ and satellite data, and on the other hand based on the output of a high-resolution ocean circulation model (NCAR). Differences will be interpreted in terms of physical signal but also in terms of error structures.

Figure 6-17 shows the annual amplitudes of the salinity tendency (ST, change in salinity per month), as well as the annual amplitude from the salinity budget terms from the model (left) and observations (including satellite and in situ data (see Köhler et al., 2018) (right).

The annual amplitude of the salinity tendency based on both the model and the CCI+SSS data shows corresponding spatial patterns with maxima in the tropics underneath the ITCZ, in river outlet regions, the high latitudes, the southern Arabian Sea, Bay of Bengal and the tropical Indian Ocean south of the equator. Outside the described regions, variability of ST is less than 0.1 per month on annual time scales. Differences between the annual amplitude of simulated and observed ST can be found in coastal regions. From Figure 6-17 it can be seen, that mainly SEF and the mean HADV resembles the spatial variability of the salinity tendency. Here, both, surface external forces (SEF) and mean horizontal advection (mean HADV) balance the ST variability on annual timescales. In general SEF shows a large seasonal amplitude, where also E-P shows a strong seasonal cycle, e.g., in the northern Bay of Bengal and in the eastern Arabian Sea, induced by enhanced monsoonal precipitation and river runoff or underneath the ITCZ.



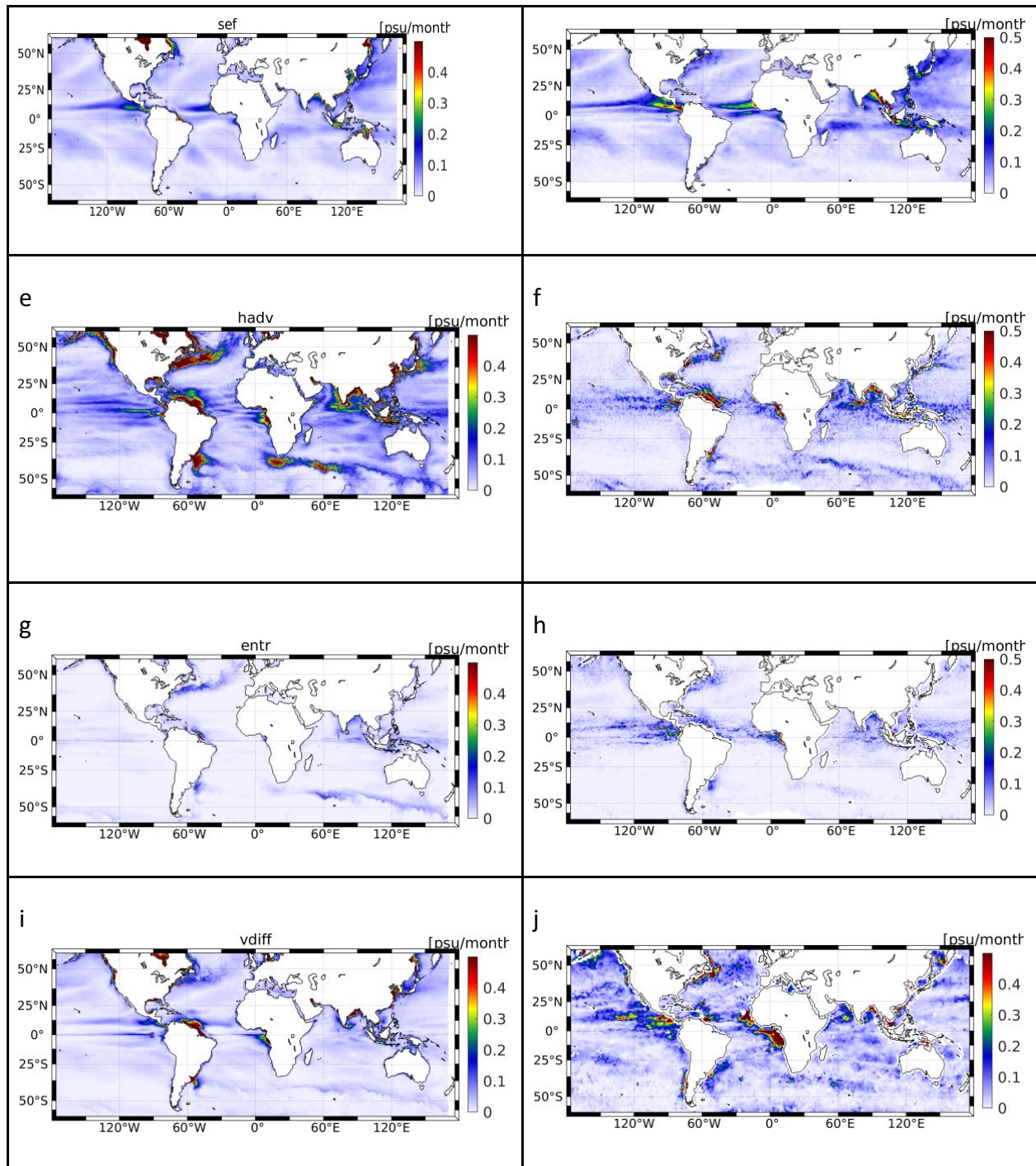


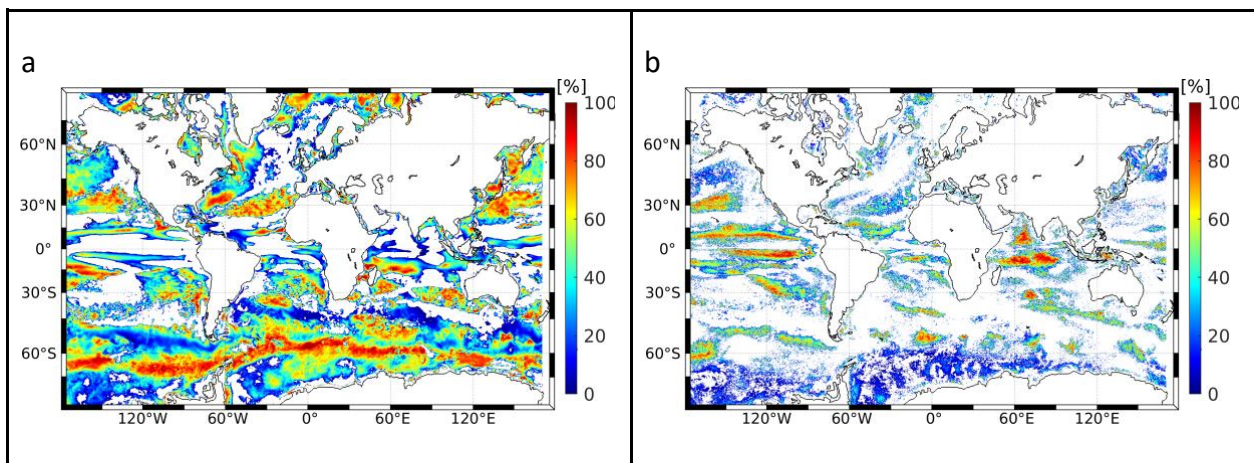
Figure 6-17: Amplitude of the annual cycle of (a, b) salinity tendency (ST), (c, d) surface external forces (SEF), (e, f) mean horizontal salinity advection (mean HADV), (g, h) entrainment (ENTR) and (i, j) vertical salinity diffusion (VDIFF), for (left) the model over the period 1980–2009 and (right) the CCI+SSS v3.2 observations in the period 2011–2019.

The observations present a stronger SEF annual cycle than the model. The ENTR term is enhanced in regions of strong vertical salinity gradients, as in the river outflow regions and frontal regions. A larger ENTR annual amplitude in the observations can be seen for example in the central Indian Ocean between 3°S and 12°S, where open ocean upwelling takes place (Schott et al., 2009). The discrepancies between model and observational ENTR south could be attributed to differences

in the temporal change of the MLD and differences in the vertical flux at the mixed-layer base, showing both larger amplitudes in the observations due to a shallower MLD in that case (not shown here). In the model, VDIFF shows a strong annual cycle in SEF-dominated regions and in the river outflow regions. The observational VDIFF shows corresponding spatial patterns with the simulation varying slightly in magnitude. A comparison of CCI+SSS v3 to v1 shows that the SEF annual cycle is less strong in the ITCZ region for v3 of the data. In the newest version rainy SSS were filtered out at level 2 using IMERG rain rate. This leads to a better accordance of the observational results with the model results. Furthermore, the ST and ADV annual cycle is less strong in this region compared to CCI+SSS v1.8 and v2.3, which is also due to the filtering at level 2 leading to a better accordance between model and observational results.

We now turn our attention to the proportion of MLS tendency explained by each budget term (Figure 6-18). SEF (Figure 6-18a) explains a large proportion of ST in regions of strong E-P annual cycle (e.g., subtropical gyres, ITCZ). The mean HADV (Figure 6-18b) largely explains ST in the southern Arabian Sea and in off-equatorial regions in the western and central Indian Ocean (between 12°S and 5°S). Interestingly, ENTR shows no large values of explained variance, but almost everywhere a proportion of around 20%, showing the importance of vertical processes for generating MLS variability. VDIFF explains lots of variability in regions where the vertical salinity gradient has a strong seasonal cycle.

The proportion of annual ST explained by the sum of SEF, mean HADV, ENTR, and VDIFF is presented in Figure 6-18e. The sum of these terms explains more than 90% in huge parts of the oceans, but the sum of the considered processes cannot explain annual ST variance, indicating that the unconsidered eddy and shear processes and/or the combination of these terms together with the unconsidered terms are of importance for closing the budget in particular regions. In summary, the spatial patterns of annual variance explained by SEF, mean HADV, ENTR, and VDIFF for model and observational cases show an overall good agreement. However, the patterns of explained ST by oceanic processes (mean HADV, ENTR, and VDIFF) differ in magnitude and in some cases location. There are contributing deficiencies from using mixed-layer averaged velocities in the MLS mean HADV term. This holds also for the assumptions regarding the vertical velocity and horizontal induction made when calculating ENTR.



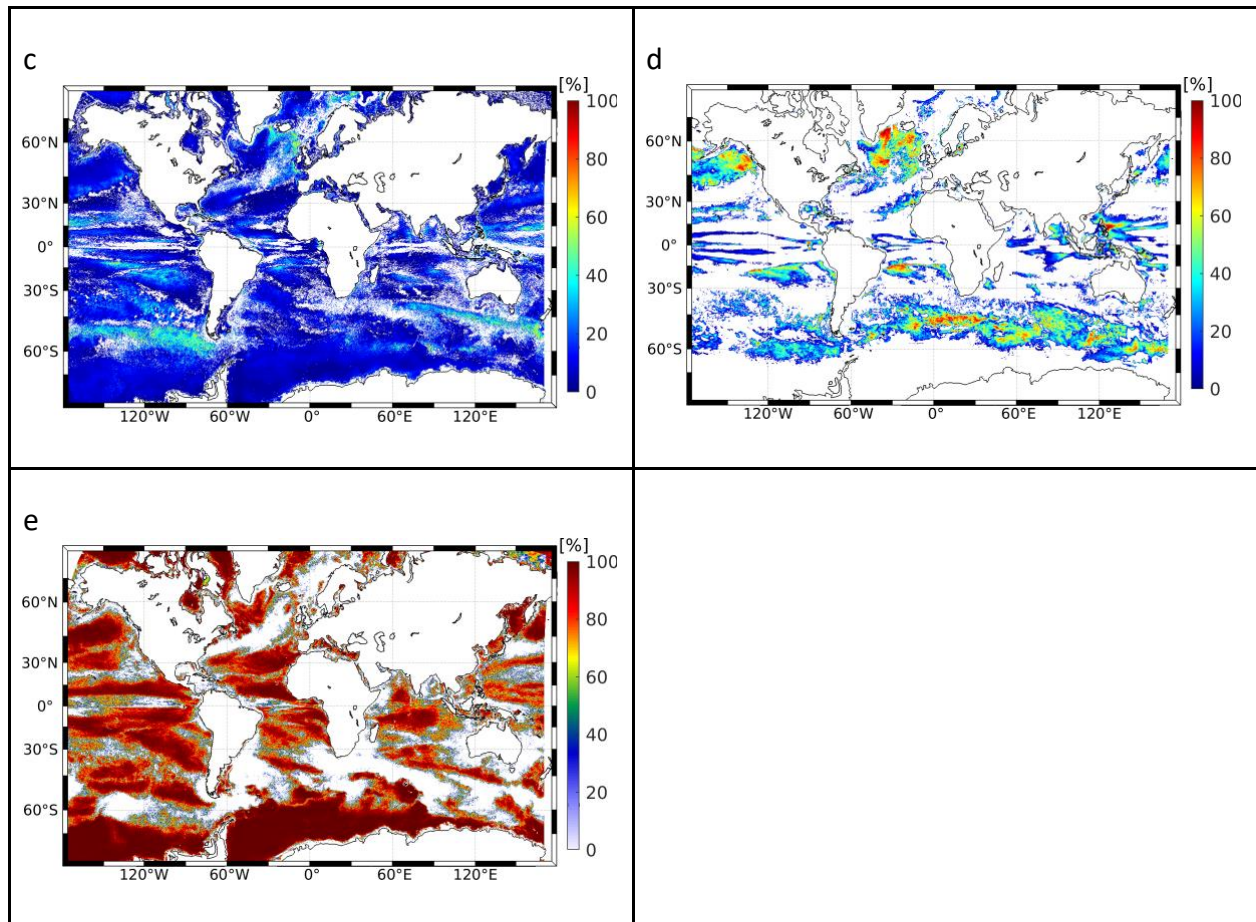


Figure 6-18: Percentage of the MLS tendency annual variance explained by (a) surface external forces (SEF), (b) mean horizontal advection (mean HADV), (c) entrainment (ENTR), (d) vertical diffusion (VDIFF) and (e) the sum of the considered terms (SEF + mean HADV + ENTR + VDIFF), using model data. Locations with explained variance less than 5% are masked white.

Next will be the analysis of the small-scale high-frequency terms and its contribution to the MLS budget. Furthermore, the analysis will be adapted to interannual and semiannual variations. The result will be a better estimate of the SSS variability on all temporal and spatial scales in addition to an estimate of the true SSS uncertainty in comparison to the errors indicated in the different data products. For a thorough investigation of the change in the global hydrological cycle and the climate variability reliable information about errors and uncertainties are indeed crucial. Furthermore, analyses of long-term SSS variability as well as their uncertainties need a thorough determination.

6.3.7 CASE STUDY 1: North Atlantic salinity anomaly

by Simon Josey, Adrien Martin, Jeremy Grist (NOC), G. Reverdin and T. Lesigne (LOCEAN)

Previous research has provided strong evidence for anomalously cold conditions in the North Atlantic subpolar gyre in 2014-16 (Josey et al., 2018). The aim of this project is to determine whether there is any corresponding signal in salinity using the ESA CCI+SSS product and alternative sources of salinity data e.g., Argo (EN4 dataset).

The initial analysis has explored the stability of the first release of the CCI+SSS dataset (CCI+SSS v1.8). Comparison of two 4-year periods (2010-13 and 2014-17) shown in Figure 6-19 has revealed an increase in salinity from 2010 through 2017 with some exceptions (Tropical Pacific). This increase is particularly strong in the North Atlantic mid-high latitudes and has been linked to RFI contamination (PVIR).

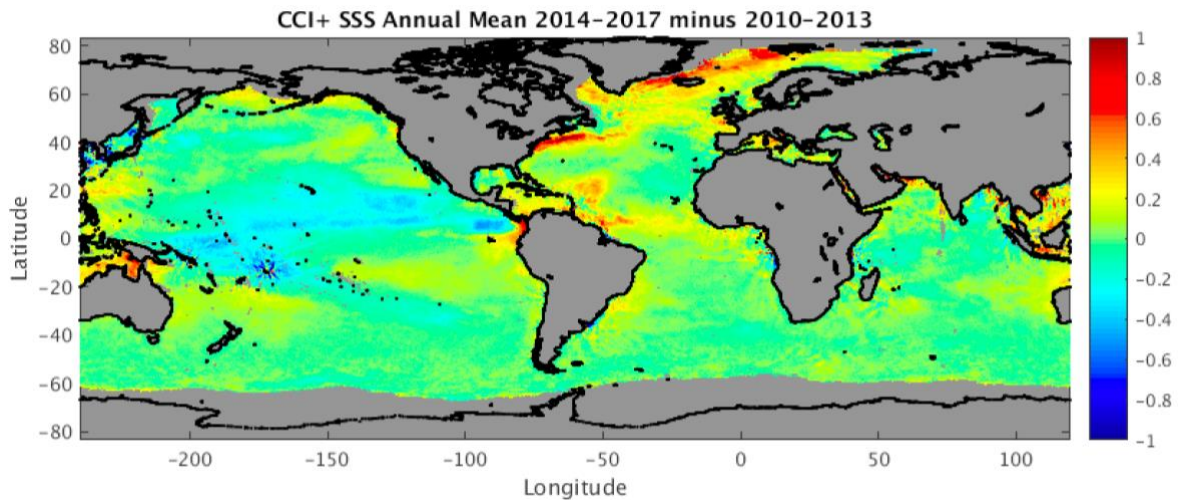


Figure 6-19 Difference of CCI+ SSS between 2014-17 and 2010-13.

A correction for the unrealistic CCI+ SSS trend has been developed using surface salinity fields from the EN4 dataset. A linear trend fit has been determined at the level of individual grid cells for EN4. The CCI - EN4 trend difference (Figure 6-20) is then removed at grid cell level to anchor CCI trends to EN4.

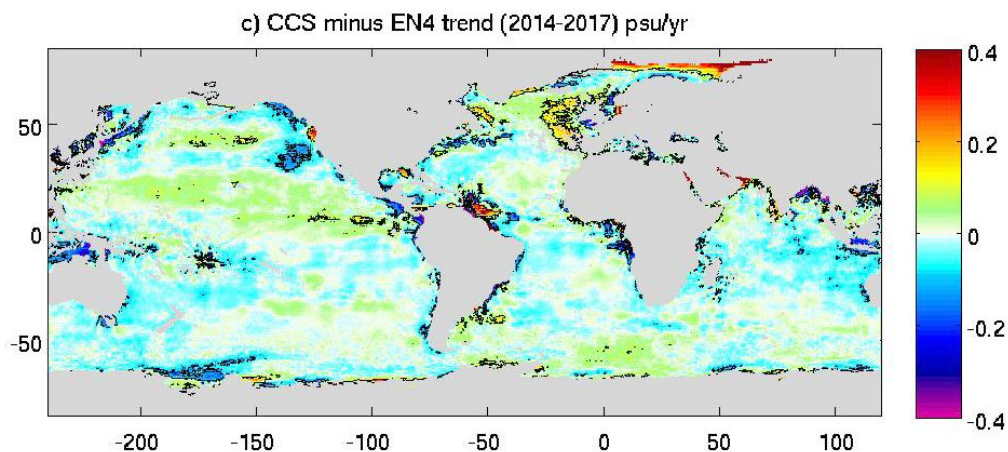


Figure 6-20: Difference of CCI+SSS linear salinity trend fields (psu/yr). Note positive values in North Atlantic mid-high latitudes.

Salinity anomalies in the North Atlantic have been determined before and after the trend adjustment process (Figure 6-21). A subpolar gyre fresh anomaly at a similar location to the

previously noted cold anomaly is partially evident in the uncorrected CCI+ SSS fields. Following anchoring of these fields to EN4 the fresh anomaly is more clearly defined.

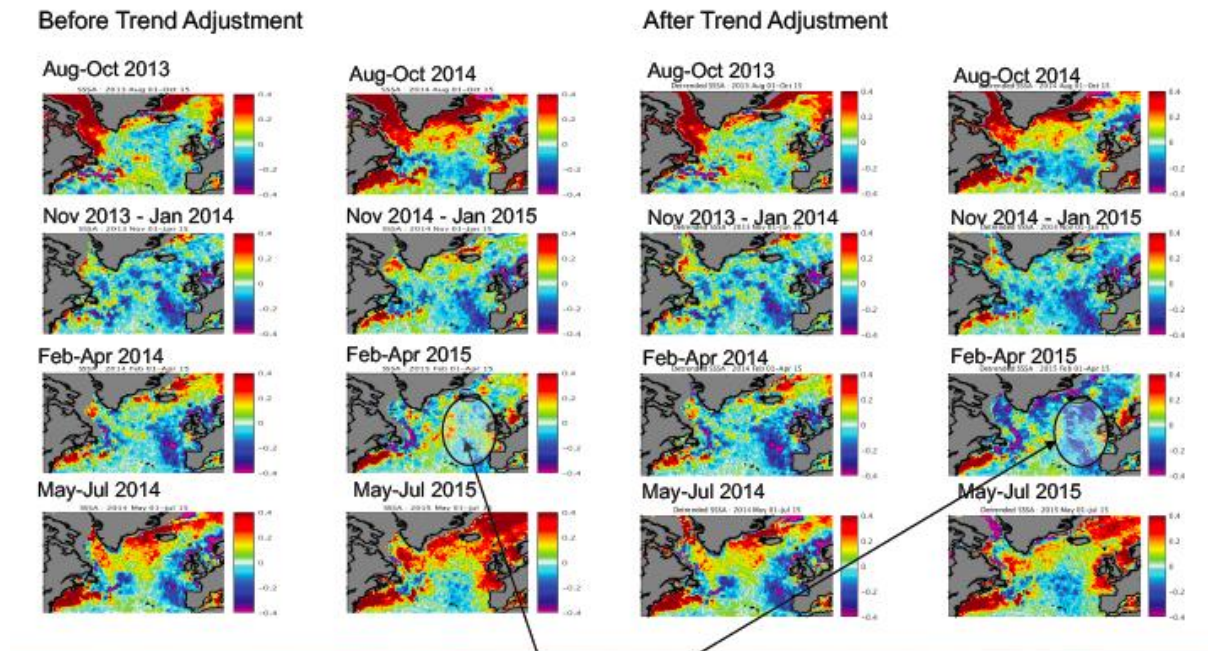


Figure 6-21: Salinity anomalies (with respect to 2010-2017) in the North Atlantic before and after the trend adjustment. Note circled fresh anomaly which is more evident following the trend correction.

Nevertheless, a serious limitation of this work is that the errors associated with RFIs do not follow a linear trend. Given that there is much less RFIs after 2012 in the northern Atlantic (as can be checked on the number of outlier field in the CCI+SSS products), future studies should try to make use of a climatology computed over a shorter period and should investigate several thresholds on the outlier field.

Ongoing work, motivated by results of Lesigne (2020, Rapport de Master, Sup. Boutin, Reverdin), is focusing on salinity anomalies in the mid-high latitude North Atlantic in 2018 and 2019, as observed on CCI+SSS v2.3 dataset. Lesigne identified a strong fresh anomaly in CCI+SSS in June 2018 with some evidence of subsequent eastward propagation (**Error! Reference source not found.**)

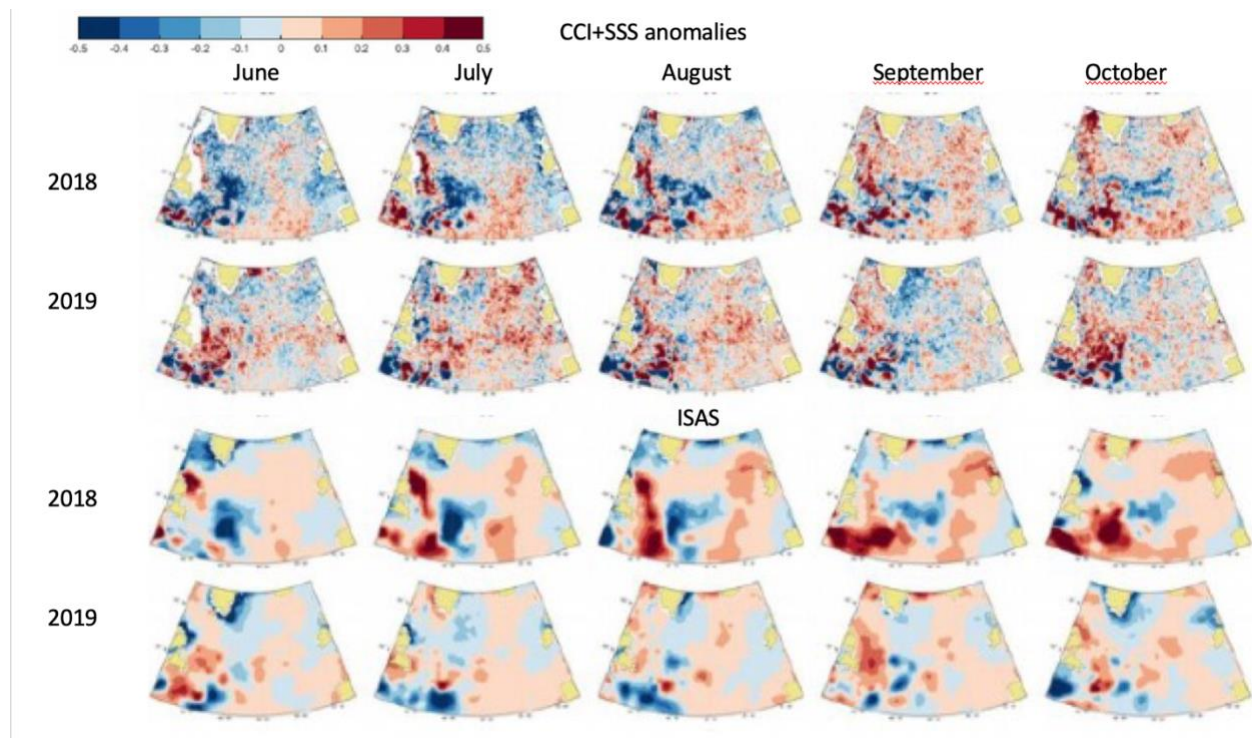


Figure 6-22: Monthly salinity anomalies relative to the monthly climatology computed from May 2015 to December 2019 in the North Atlantic for June, July and August, September and October 2018 and 2019 for (upper two rows) CCI+SSS and (lower two rows) ISAS.

Anomalies for the same month based on ISAS are also shown in Figure 6-22 showing corresponding patterns, but smoother. Analysis of EN4.2.1 data reveals similar anomalies in the surface layer (0-10 m) salinity but slightly differs from the satellite SSS and ISAS anomalies, showing the need for having a long time series to get an adequate reference climatology. The CCI+SSS and ISAS anomalies are relative to a monthly climatology computed from May 2015 to 2019, whereas the EN4.2.1 anomalies are relative to a monthly climatology based on a 30-year period.

Anomaly signal weakens but is still present at the end of 2018 following an eastward propagation (Figure 6-23 e.g., compare July and December 2018). The 2018 fresh anomaly is still present through to June 2019 (compare **Error! Reference source not found.**) but weakens considerably. As observable from Figure 6-6 a new fresh anomaly develops in July 2019 around 40°N propagating north-eastward during the second half of the year.

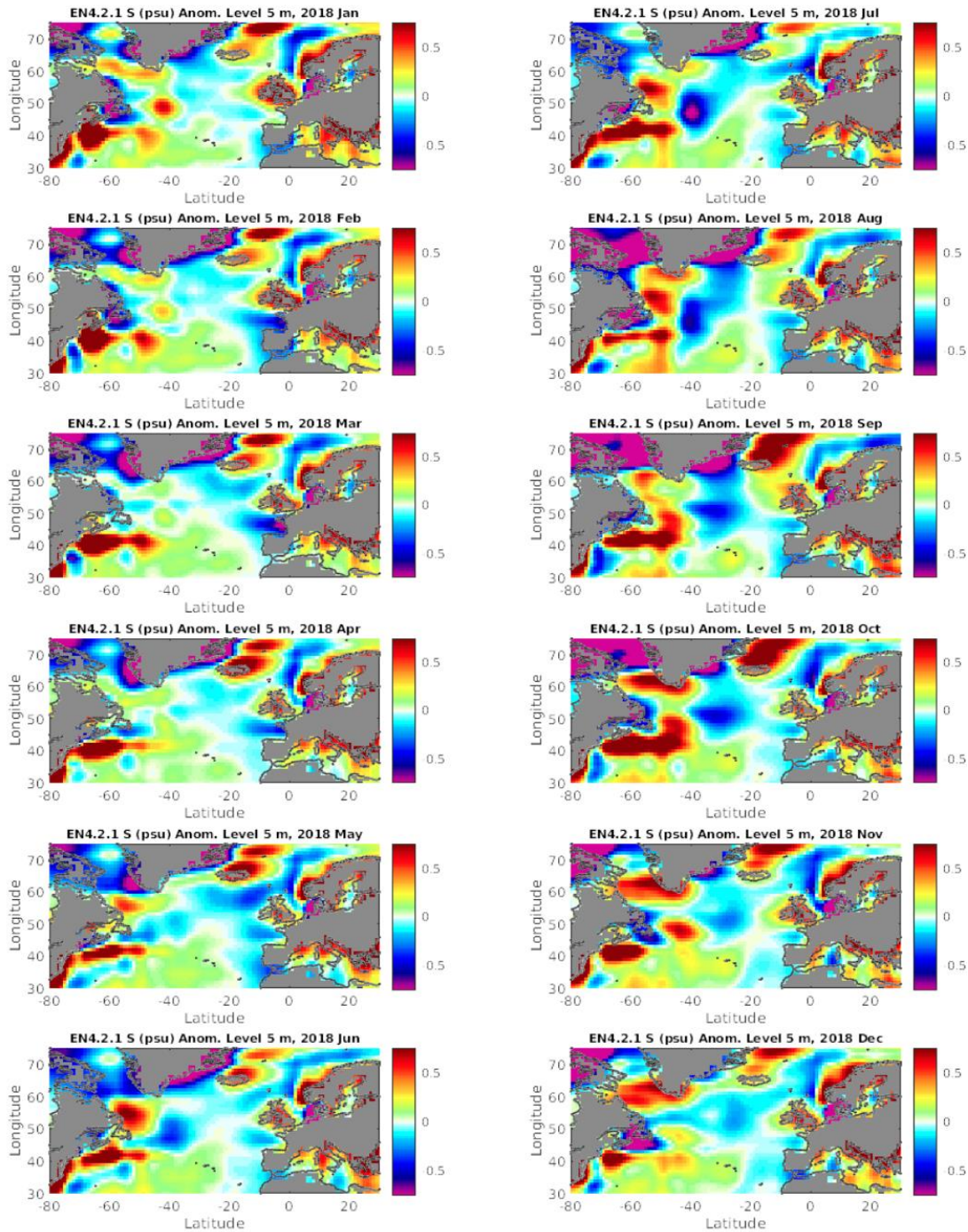


Figure 6-23: Monthly EN4.2.1 salinity anomalies (with respect to 1981-2010) in the North Atlantic in 2018.

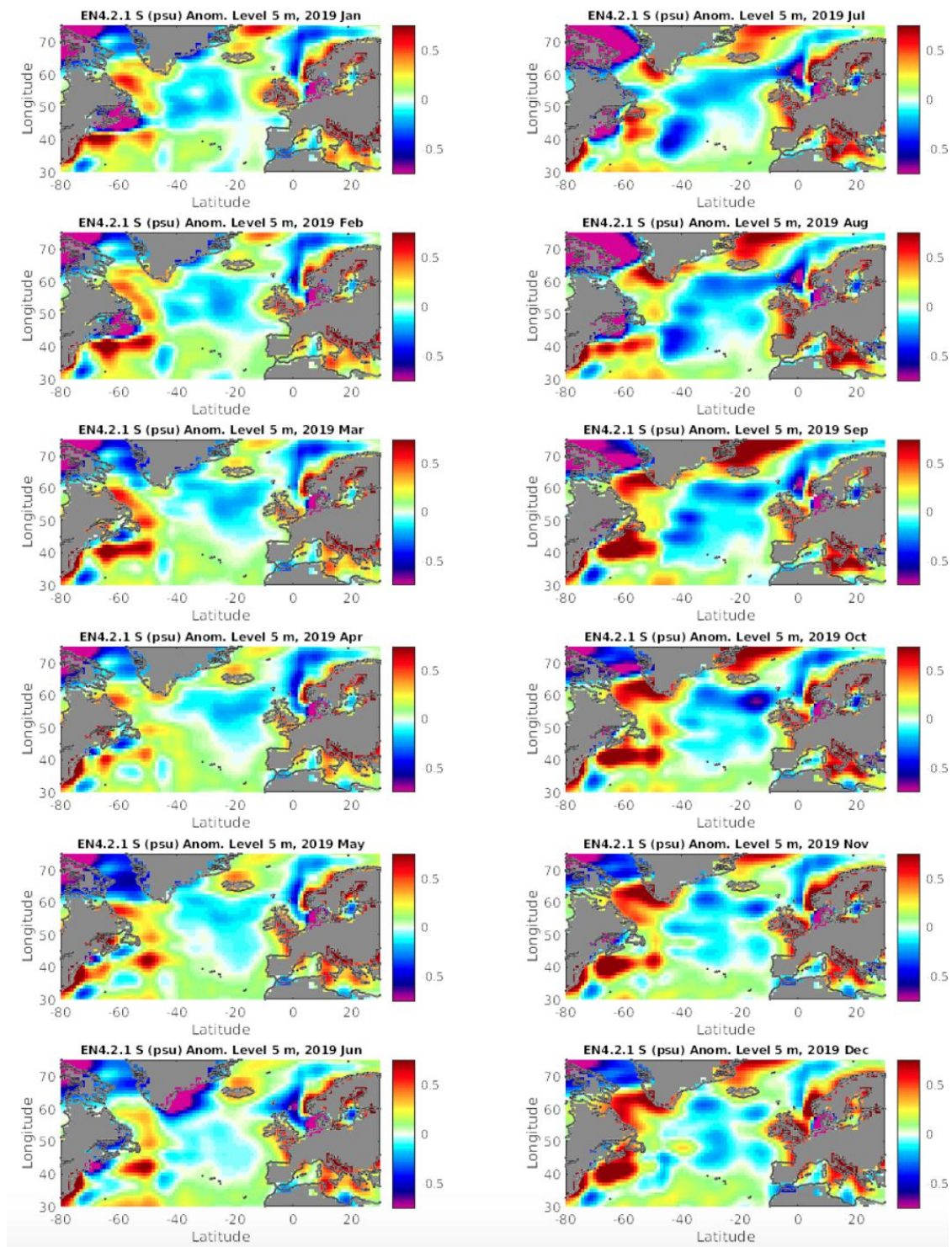


Figure 6-24: Monthly EN4.2.1 salinity anomalies (with respect to 1981-2010) in the North Atlantic in 2019.

To investigate if the observed fresh anomaly patterns are part of a larger gyre wide freshening, the variation of the anomaly with depth is explored using a Hovmöller analysis at five points along the anomaly track.

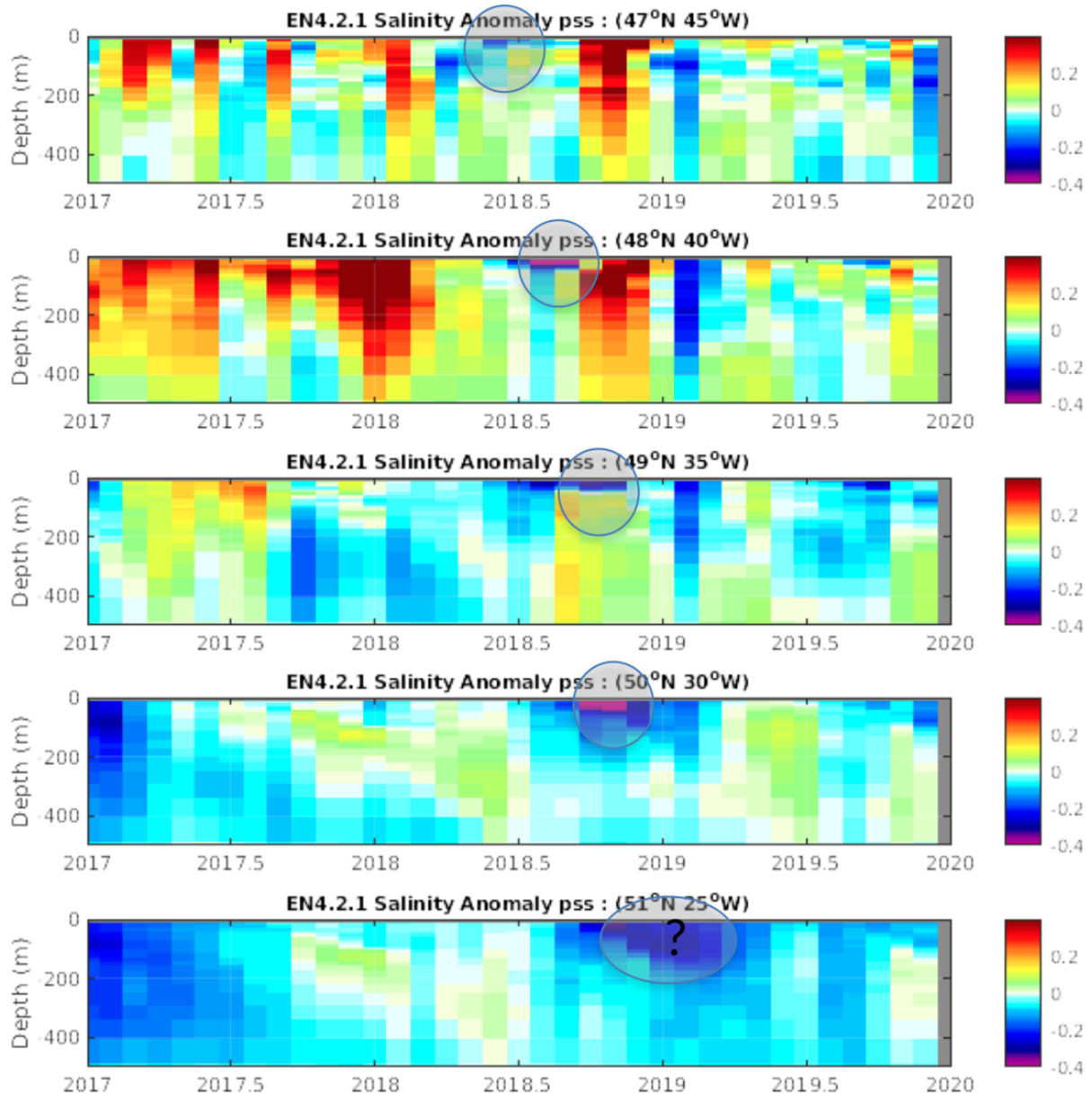


Figure 6-25: Hovmöller diagram showing EN4.2.1 monthly salinity anomaly at 5 points along the propagation track.

From Figure 6-25 it can be seen that there is a strong signal confined to the top 30-40 m in May 2018 at 47°N and 45°W.

The anomaly may reinforce and extend to greater depths as it propagates, indicated by the strong anomaly pattern at 51°N and 25°W in the first half of the year 2019. It's not clear yet, if this may be a combination of two separate anomalies. Ongoing work will employ the next release of the

CCI+ SSS fields that will extend over a longer period (up to 2019), bringing them together with subsurface salinity data and examine the relationship between the fresh anomaly and potential causative mechanisms, including changes in the air-sea freshwater exchange.

6.3.8 Amazon river plume

By L. Macarez

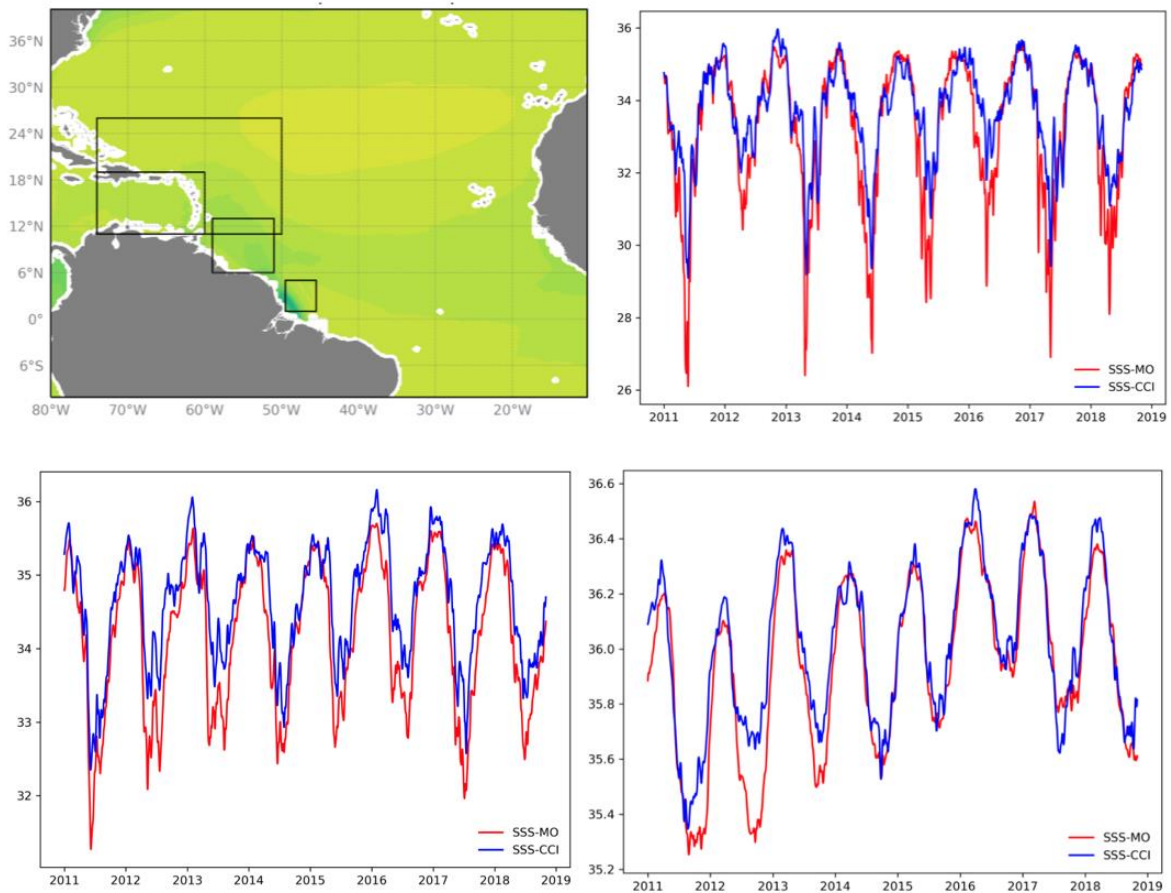


Figure 6-26 : Time series of the mean Sea Surface Salinity in different boxes along the path of the Amazon river plume, in red the Mercator Ocean global 1/12° analysis and in blue the ESA CCI+ weekly L4 SSS (v1.8). Top right panel: mean SSS in the small box close to the river mouth, bottom left panel in the second box (6°N-13°N) and bottom right panel in the largest box covering the Caribbean archipelago.

A comparison between the Mercator Ocean operational sea surface salinity analysis at 1/12° and the ESA CCI+ SSS L4 weekly products (v1.8, doi: 10.5285/9ef0ebf847564c2eabe62cac4899ec41) was conducted over the period from 2011 to 2018. The focus was on the variability of the SSS in the Amazon River plume area. This comparison has shown an overall good agreement between the analysis produced by the global 1/12° real time system and the ESA CCI+SSS observations. On the continental shelf, where more complex physical processes occur (not always represented in the model) and the observations are less accurate, the agreement was not as good. This can be seen on Figure 6-26 showing the time series of the mean SSS in several boxes from the Amazon River mouth to the Caribbean archipelago. The phasing of the variability is very coherent

between the analysis and the observations, but the minimum value of salinity is much lower in the global model system on the shelf. The prescribed runoff in the Mercator system is climatological and may be too strong, another possible reason for the disagreement close to the coast is the absence of the tide in the model.

(Results and figures from Lynne Macarez internship at Mercator Ocean)

6.3.9 SSS signatures related to ENSO

By A. Hasson et al.

Figure 6-27 shows the CCI+SSS longitude variability related warm pool and equatorial upwelling spatial-temporal variations. This is an update by A. Hasson of the Figure 10 that is in Popp, T., M. I. Hegglin, R. Hollmann, F. Arduin, A. Bartsch, A. Bastos, V. Bennett, J. Boutin, et al., Consistency of satellite climate data records for Earth system monitoring, Bull. Amer. Meteor. Soc., <https://doi.org/10.1175/BAMS-D-19-0127.1> (2020). The ocean and most atmosphere ECV time series show consistent spatial-temporal co-variability, as expected. CCI+SSS performs well in showing the ENSO related variability in the Pacific, highlighting the remarkable extension and contraction of the freshwater pool in relation to the El Niño or La Niña periods.

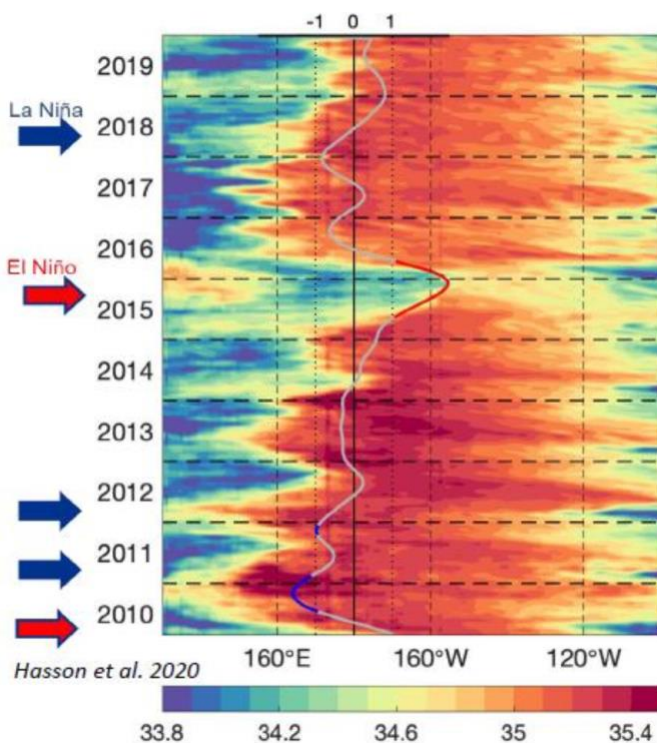


Figure 6-27 Zonal month-longitude cross sections (averaged 5°S and 5°N) for Sea Surface Salinity (CCI+SSS v2.3)



7 Summary and next steps

In this climate assessment report, we have presented five case studies and additional studies undertaken to evaluate the quality of CCI+SSS products and their efficiency for climate studies. We summarized the key results of the product validation against in situ observations (more details in PVIR) and highlighted the improvement of the multi-satellite product against previous single-satellite SSS products. We provided examples of the use of sea surface salinity data for climate/variability studies to understand the impact of periodicity on various timescales in the data. Combining in situ and satellite-retrieved salinity data to analyse salinity budgets provide a good overview about underlying mechanisms of salinity changes on a global scale. Analysis of salinity variability based on the newest version of the dataset (v3.2) shows an improvement of patterns and magnitudes compared to in situ or model data and compared to the first version of the data set. The flagging of data in coastal regions is less stringent and SSS variability in v3.2 underneath the ITCZ is reduced compared to v1.8 due to the filtering of data in rainy regions at level 2. These changes lead to promising results in comparison with the output of a high resolution model, showing reduced differences in magnitudes of the variability. Nevertheless, salinity variability analysis in specific regions, like near coastal regions, remain challenging due to sparse in situ data coverage and higher uncertainties of the satellite data. Here, basic research still needs to be done to get a clearer picture of the salinity variability in these regions. It becomes clear that we need longer time series to get an adequate climatology and to analyse interannual variabilities, trends and climate impacts.

We have already achieved a lot in improving algorithms and developing unique products to meet user requirements, more will be done in the second phase of the project. The usage of data from additional sensors (e.g., AMSR-E) has to be considered to ensure an adequate length of time series in the high-variable river plume regions.

The broad user community provided strong support, by responding to requests and giving feedback to the data and the caveats. This shows the importance of maintaining user consultation and to continue to develop the products to meet the user requirements even better.

In addition to the points mentioned above, further steps for the second phase of the project are a closer collaboration with CMUG to define user requirements suitable for Earth observation scientists and modellers, to strongly motivate for the usage of CCI+SSS data in modelling studies outside of validation and to perform a modelling science study within the frame of the CCI+SSS project.

8 References

Akhil, V.P., J. Vialard, M. Lengaigne, M.G. Keerthi, J. Boutin, J.-I. Vergely and F. Papa, 2020: Bay of Bengal Sea surface salinity variability using a decade of improved SMOS re-processing, *Rem. Sens. Envir.*, 248, doi: <https://doi.org/10.1016/j.rse.2020.111964>

Akhil, V.P., F. Durand, M. Lengaigne, J. Vialard, M.G. Keerthi, V.V. Gopalakrishna, C. Deltel, F. Papa and C. de Boyer Montégut, 2014: A modeling study of the processes of surface salinity seasonal cycle in the Bay of Bengal, *J. Geophys. Res. Oceans*, 119, doi:10.1002/2013JC009632.

Akhil, V. P., M. Lengaigne, J. Vialard, F. Durand, M. G. Keerthi, A. V. S. Chaitanya, F. Papa, V. V. Gopalakrishna, and C. de Boyer Montégut, 2016a: A modeling study of processes controlling the Bay of Bengal sea surface salinity interannual variability, *J. Geophys. Res. Oceans*, 121, 8471–8495, doi:10.1002/2016JC011662.

Akhil, V.P., M. Lengaigne, F. Durand, J. Vialard, V.V. Gopalakrishna, C. de Boyer Montégut and J. Boutin, 2016b: Validation of SMOS and Aquarius remotely-sensed surface salinity in the Bay of Bengal, *IJRS*, 37, doi: 10.1080/01431161.2016.1145362

Boutin J., J.L. Vergely, S. Marchand, F. D'Amico, A. Hasson, N. Kolodziejczyk, N. Reul, G. Reverdin and J. Vialard (2018): New SMOS Sea Surface Salinity with reduced systematic errors and improved variability. *Remote sensing of the Environment*, 214, 115-134. doi:10.1016/j.rse.2018.05.022.

Boutin et al. (2021): Satellite-based Time-Series of Sea Surface Salinity designed for Ocean and Climate Studies (submitted to *JGR-Ocean*) doi:10.1002/essoar.10507337.1.

Callies, J., and R. Ferrari, (2013), Interpreting energy and tracer spectra of upper-ocean turbulence in the submesoscale range (1–200 km), *J. Phys. Oceanogr.*, 43, 2456–2474, doi:10.1175/JPO-D-13-063.1.

Camara, I., N. Kolodziejczyk, J. Mignot, A. Lazar, and A. T. Gaye (2015), On the seasonal variations of salinity of the tropical Atlantic mixed layer, *J. Geophys. Res. Oceans*, 120, 4441–4462, doi:10.1002/2015JC010865.

Chaitanya, A.V.S., M. Lengaigne, J. Vialard, V.V. Gopalakrishna, F. Durand, Ch. Krantikumar, V. Suneel, F. Papa and M. Ravichandran, 2014: Fishermen-operated salinity measurements reveal a “river in the sea” flowing along the east coast of India, *Bull. Am. Met. Soc.*, 95, 1897-1908.

Chelton, D. B., R. A. de Szoeke, and M. G. Schlax (1998), Geographical variability of the first Rossby baroclinic radius of deformation, *J. Phys. Oceanogr.*, 28, 433–460.

Chelton, D. B., Wentz, F. J., Gentemann, C. L., de Szoeke, R. A., & Schlax, M. G. (2000). Satellite microwave SST observations of transequatorial tropical instability waves. *Geophysical Research Letters*, 27(9), 1239–1242.



Chen et al., 2017

Counillon, F., Keenlyside, N., Bethke, I., Wang, Y., Billeau, S., Shen, M. L., & Bentsen, M. (2016). Flow-dependent assimilation of sea surface temperature in isopycnal coordinates with the Norwegian Climate Prediction Model. *Tellus, Series A: Dynamic Meteorology and Oceanography*, 68(1), 1–17.

Da-Allada, C. Y., G. Alory, Y. du Penhoat, E. Kestenare, F. Durand, and N. M. Hounkonnou (2013), Seasonal mixed-layer salinity balance in the tropical Atlantic Ocean: Mean state and seasonal cycle, *J. Geophys. Res. Oceans*, 118, 332–345, doi:10.1029/2012JC008357.

Estella-Perez, V., Mignot, J., Guilyardi, E., Swingedouw, E., and Reverdin, G. Advances in Reconstructing the AMOC using Sea Surface Observations of Salinity. Under review for *Climate Dynamics*.

Felton, C. S., Subrahmanyam, B., Murty, V. S. N., and Shriver, J. F. (2014), Estimation of the barrier layer thickness in the Indian Ocean using Aquarius Salinity, *J. Geophys. Res. Oceans*, 119, 4200–4213, doi:[10.1002/2013JC009759](https://doi.org/10.1002/2013JC009759).

Fournier, S., Vialard, J., Lengaigne, M., Lee, T., Gierach, M. M., & Chaitanya, A.V. S., 2017: Modulation of the Ganges-Brahmaputra river plume by the Indian Ocean dipole and eddies inferred from satellite observations. *Journal of Geophysical Research: Oceans*, 122, 9591–9604. <https://doi.org/10.1002/2017JC013333>

Fox-Kemper, B., R. Ferrari, and R. Halberg (2008), Parametrization of the mixed layer eddies. Part I: Theory and diagnosis, *J. Phys. Oceanogr.*, 38(6), 1145–1165.

Friedman, A. R., G. Reverdin, M. Khodri, and G. Gastineau (2017), A new record of Atlantic sea surface salinity from 1896 to 2013 reveals the signatures of climate variability and long-term trends, *Geophys. Res. Lett.*, 44, 1866–1876,

Houdegnonto, O.J., N. Kolodziejczyk, C. Maes, B. Bourlès, C. Da-Allada, and N. Reul: Seasonal variability of the Gulf of Guinea fresh water plumes. *Journal of Geophysical Research: Ocean*. <https://doi.org/10.1029/2020JC017041>

Josey, S. A., J. J.-M. Hirschi, B. Sinha, Duchez, A., J. P. Grist and R. Marsh, 2018: The Recent Atlantic Cold Anomaly: Causes, Consequences and Related Phenomena, *Annual Reviews of Marine Science*, doi.org/10.1146/annurev-m

Kilpatrick, K. A., G. Podestá, S. Walsh, E. Williams, V. Halliwell, M. Szczodrak, O. B. Brown, P. J. Minnett, and R. Evans (2015). A decade of sea surface temperature from MODIS. *Remote Sensing of Environment*, 165, 27-41. <http://dx.doi.org/10.1016/j.rse.2015.04.023>.

Kolodziejczyk, N., O. Hernandez, J. Boutin, and G. Reverdin (2015), SMOS salinity in the subtropical north Atlantic salinity maximum. Part II: Horizontal thermohaline variability, *J. Geophys. Res. Oceans*, 120, 972–987, doi:10.1002/2014JC010103.

Kolodziejczyk, N., G. Reverdin, J. Boutin, and O. Hernandez (2015), Observation of the surface horizontal thermohaline variability at mesoscale to submesoscale in the north-eastern subtropical Atlantic Ocean, *J. Geophys. Res. Oceans*, 120, doi:10.1002/2014JC010455.

Köhl, A., D. Stammer, and M. Sena-Martins, 2014: Impact of Assimilating Surface Salinity from SMOS on Ocean Circulation Estimates. *J. Geophysical Res.*, 119, 5449– 5464, doi: 10.1002/2014JC010040.

Köhler, J., N. Serra, F. Bryan, B. K. Johnson and D. Stammer, 2018: Mechanisms of Mixed-Layer Salinity Seasonal Variability in the Indian Ocean, *J. Geophys Res.*,

Lee, T., Lagerloef, G., Kao, H.-Y., McPhaden, M. J., Willis, J., & Gierach, M. M. (2014). The influence of salinity on tropical Atlantic instability waves. *Journal of Geophysical Research: Oceans*, 119(12), 8375–8394. <https://doi.org/10.1002/2014JC010100>

Lesigne, T., 2020: Study of the variability of surface salinity measured by satellite and in situ in the North Atlantic Ocean from 2010 to 2020, Master 1 Sciences de l'océan, de l'atmosphère et du climat, Sorbonne University, 2020.

Levy, M., and A. P. Martin (2013), The influence of mesoscale and submesoscale heterogeneity on ocean biogeochemical reactions, *Global Biogeochem. Cycles*, 27, doi:10.1002/2012GB004518

Liu, X. et al., 2016. Impact of in-consistency between the climate model and its initial conditions on climate prediction. *Climate Dynamics*.

Mignot, J., García-Serrano, J., Swingedouw, D. et al. *Clim Dyn* (2016) 47: 1225. <https://doi.org/10.1007/s00382-015-2898-1>

Olivier, L., G. Reverdin, A. Hasson, and J. Boutin (2020), Tropical Instability Waves in the Atlantic Ocean: Investigating the Relative Role of Sea Surface Salinity and Temperature From 2010 to 2018, *Journal of Geophysical Research: Oceans*, 125(12), e2020JC016641, doi:<https://doi.org/10.1029/2020JC016641>.

Ortega P., E Guilyardi, D. Swingedouw, J. Mignot, S. Nguyen (2017). Reconstructing extreme AMOC events through nudging of the ocean surface: A perfect model approach. *Clim. Dyn.* doi:10.1007/s00382-017-3521-4

Ray, S. et al., 2015. Effect of surface restoring on subsurface variability in a climate model during 1949-2005, *Climate Dynamics*, 44(9–10), pp.2333–2349.

Reul, N., B. Chapron, T. Lee, C. Donlon, J. Boutin, and G. Alory (2014), Sea Surface Salinity structure of the meandering Gulf Stream revealed by SMOS sensor, *Geophys. Res. Lett.*, 41, 3141–3148, doi:10.1002/2014GL059215.



Reverdin, G., E. Kestenare, C. Frankignoul, T. Delcroix, 2007. In situ surface salinity in the tropical and subtropical Atlantic Ocean. Part I. Large scale variability. *Progress in Oceanogr.*, 73, 3, 311-340.

Reverdin, G., et al. (2021), Formation and Evolution of a Freshwater Plume in the Northwestern Tropical Atlantic in February 2020, *Journal of Geophysical Research: Oceans*, 126(4), e2020JC016981, doi:10.1029/2020jc016981.

Schlundt, M., Brandt, P., Dengler, M., Hummels, R., Fischer, T., Bumke, K., Krahnemann, G., and Karstensen, J. (2014), Mixed layer heat and salinity budgets during the onset of the 2011 Atlantic cold tongue, *J. Geophys. Res. Oceans*, 119, 7882–7910, doi:[10.1002/2014JC010021](https://doi.org/10.1002/2014JC010021).

Schiller, A., and Oke, P. R. (2015). Dynamics of ocean surface mixed layer variability in the Indian Ocean. *J. Geophys. Res. Ocean.* 120, 4162–4186. doi: 10.1002/2014JC010538

Sena Martins, M., N. Serra, and D. Stammer, 2015: Sea surface salinity variability in the Atlantic Ocean. *J. Geophys. Res.*, 120, 4306-432, 3 DOI: 10.1002/2014JC010649.

Servonnat, J. et al., 2014. Reconstructing the subsurface ocean decadal variability using surface nudging in a perfect model framework. *Climate Dynamics*.

Sepulchre et al., submitted. IPSL-CM5A2. An Earth System Model designed for multi-millennial climate simulations. *Geoscientific Model Development (GMD)*.

Stammer, D., M. Sena Martins, J. Köhler and A. Köhl, 2021: How well do we know ocean salinity and its changes?. *Progress in Oceanography*

Swingedouw, D. et al., 2013. Initialisation and predictability of the AMOC over the last 50 years in a climate model. *Climate Dynamics*, 40(9–10), pp.2381–2399.

Wilson, E. A., & Riser, S. C., 2016. An assessment of the seasonal salinity budget for the upper Bay of Bengal. *Journal of Physical Oceanography*, 46, 1361–1376.

Yeager, S. G., & Robson, J. I. (2017). Recent Progress in Understanding and Predicting Atlantic Decadal Climate Variability. *Current Climate Change Reports*, 3(2), 112–127.



Climate Change Initiative+ (CCI+)
Phase 1
Climate Assessment Report

Ref.: ESA-CCI-PRGM-EOPS-SW-17-0032
Date: 08/11/2021
Version : v3.2
Page: 73 of 75

End of document



Climate Change Initiative+ (CCI+)
Phase 1
Climate Assessment Report

Ref.: ESA-CCI-PRGM-EOPS-SW-17-0032
Date: 08/11/2021
Version : v3.2
Page: 1 of 75

Annex 1

End of document